Predictive Control of HCCI Engines Using Physical Models

Widd, Anders

2009

Document Version:
Publisher's PDF, also known as Version of record

Link to publication

Citation for published version (APA):
Widd, A. (2009). *Predictive Control of HCCI Engines Using Physical Models*. [Licentiate Thesis, Department of Automatic Control]. Department of Automatic Control, Lund Institute of Technology, Lund University.

Total number of authors:
1

Predictive Control of HCCI Engines using Physical Models

Anders Widd

Department of Automatic Control
Lund University
Lund, May 2009

Abstract

Homogeneous Charge Compression Ignition (HCCI) is a promising internal combustion engine concept. It holds promise of combining low emission levels with high efficiency. However, as ignition timing in HCCI operation lacks direct actuation and is highly sensitive to operating conditions and disturbances, robust closed-loop control is necessary. To facilitate control design and allow for porting of both models and the resulting controllers between different engines, physics-based mathematical models of HCCI are of interest.

This thesis presents work on a physical model of HCCI including cylinder wall temperature and evaluates predictive controllers based on linearizations of the model. The model was derived using first principles modeling and is given on a cycle-to-cycle basis. Measurement data including cylinder wall temperature measurements was used for calibration and validation of the model. A predictive controller for combined control of work output and combustion phasing was designed and evaluated in simulation. The resulting controller was validated on a real engine. The last part of the work was an experimental evaluation of predictive combustion phasing control. The control performance was evaluated in terms of response time and steady-state output variance.

Acknowledgements

Contents

1

Introduction

1.1 Motivation

The goal of most engine research is to reduce the emissions and the fuel consumption of transportation. While some emissions, such as nitrogen oxides and soot, are immediately harmful to humans and the local environment, carbon dioxide emissions are receiving increased attention due to the ongoing discussions about climate change. Various after-treatment systems for reducing the harmful emissions are available. However, after-treatment systems for diesel engines, such as particulate filters and selective catalytic reduction (SCR) are typically expensive. Also, in order to reduce the emissions of carbon dioxide, the engine efficiency must be increased, so that less fuel is consumed for a specific amount of produced work. By altering the combustion mode both issues can be improved upon simultaneously.

Homogeneous Charge Compression Ignition (HCCI) is one of several possible technologies for future engines since it holds promise for reduced emissions and increased efficiency compared to conventional combustion engines. However, as HCCI lacks a direct combustion trigger, such as the spark in gasoline engines or the fuel injection event in diesel engines, it is more challenging to control. To this end, mathematical models aimed at control design are of interest. Engine modeling involves several disciplines such as thermodynamics, chemical combustion kinetics, and mechanics. Capturing all of these aspects in detail

typically results in large models of high complexity. To allow for fast simulation and analysis, models of lower complexity are needed.

Several methods have been evaluated for HCCI control. In [Bengtsson, 2004], similar closed-loop performance in certain operating conditions was demonstrated using PID, Linear Quadratic, and Model Predictive controllers based on identified models. From a tuning perspective, however, the ability to enforce explicit constraints on the control signals using Model Predictive Control, is advantageous [Maciejowski, 2002]. The majority of the actuators available for HCCI control have amplitude constraints and rate constraints are not uncommon for the control variables that include some form of mass flow.

1.2 Contributions of the Thesis

The model presented in this thesis is cycle-resolved, physics-based, and includes cylinder wall temperature dynamics. The cylinder wall temperature has a considerable effect on the combustion phasing when the engine is run with small amounts of trapped residuals [Blom *et al.*, 2008; Wilhelmsson *et al.*, 2005]. The continuous heat transfer between the cylinder wall and the gas charge is approximated by three heat transfer events during each cycle. This allows the model to capture the time constant of the wall temperature while keeping the complexity of the resulting model at a tractable level.

A simulation-based study of Model Predictive Control (MPC) of the ignition timing and the indicated mean effective pressure based on linearizations of the model was then performed. The model was reformulated to allow state feedback to be used. The considered control signals were the crank angle of inlet valve closing and the intake temperature. A Linear Parameter Varying (LPV) formulation of the model was found to improve the control results. An extended model formulation was introduced to handle slow dynamics in the heater that governed the intake temperature. Initial experimental results were included which showed qualitative agreement with the simulated results.

In the last part of the work, the controller was reformulated to govern only the combustion phasing. To obtain fast intake temperature actuation, a system for Fast Thermal Management (FTM) was installed and controlled using mid-ranging control. The performance of the con-

troller was then experimentally investigated in terms of response time and output variance. It was found that changing linearization point yielded a comparable reduction in output variance as did disturbance modeling in certain operating points. The computational burden of increasing the prediction and control horizons was also evaluated while monitoring the control performance. With the current model formulation and experimental setup, no noticeable increase in control performance was achieved by increasing the prediction horizons. This is promising as it suggests that satisfactory control performance can be obtained with a fairly small computational effort. Initial multi-cylinder control results were also presented.

1.3 Publications

The thesis is based on the following publications.

Widd, A., P. Tunestål, C. Wilhelmsson, and R. Johansson (2008a): "Control-oriented modeling of homogeneous charge compression ignition incorporating cylinder wall temperature dynamics." In *Proc. 9th International Symposium on Advanced Vehicle Control*. Kobe, Japan, pp. 146-151.

The current author derived the model and wrote the paper.

Widd, A., P. Tunestål, and R. Johansson (2008b): "Physical modeling and control of homogeneous charge compression ignition (HCCI) engines." In *Proc. 47th IEEE Conference on Decision and Control*. Cancun, Mexico, pp. 5615-5620.

The current author performed the control design and the simulations and wrote the paper. The experimental results were obtained in collaboration with Kent Ekholm.

Widd, A., K. Ekholm, P. Tunestål, and R. Johansson (2009): "Experimental evaluation of predictive combustion phasing control in an HCCI engine using fast thermal management and VVA." In *Proc. 18th IEEE Conference on Control Applications*. St. Petersburg, Russia. Accepted for publication.

The experiments were performed in collaboration with Kent Ekholm, who also designed the Fast Thermal Management system. The current author performed the analysis and wrote the paper.

Other Publications

Wilhelmsson, C., P. Tunestål, A. Widd, R. Johansson, and B. Johansson (2009): "A physical two-zone NO_x model intended for embedded implementation." *SAE 2009-01-1509.*

1.4 Thesis Outline

Chapter 2 gives a background to HCCI engines and the need for closed-loop control. The experimental facilities are briefly described in Chapter 3. The model and calibration results are presented in Chapter 4. A few topics related to control design are discussed in Chapter 5. The simulation-based study of combined control of combustion phasing and indicated mean effective pressure is presented in Chapter 6 and the experimental study is presented in Chapter 7. The thesis concludes with suggestions for future work in Chapter 8. A list of used symbols and acronyms is given at the end of the thesis.

2

Background

2.1 Emissions and Internal Combustion Engines

The main emissions generated by internal combustion engines are carbon monoxide (CO), carbon dioxide (CO_2), nitrogen oxides (NO_x), hydrocarbons (HC), and particulate matter [Heywood, 1988]. Of these emissions, only CO_2 is not regulated. These emissions can, to varying extent, be reduced by altering the combustion mode. The formation of NO_x is heavily dependent on the charge temperature, making engine concepts with lower in-cylinder temperatures preferable. Particulate matter, on the other hand, is mainly formed in zones with high fuel concentration. A more homogeneous mixture reduces the occurrence of these zones, and thus the formation of particulate matter.

Conventional internal combustion engines include Otto- and Diesel-engines. To simplify understanding of the Homogeneous Charge Compression Ignition principle, a brief review of these modes is given in the following sections. For further details see, e.g., [Heywood, 1988].

SI Engines

Spark Ignition (SI) engines are based on the Otto cycle. In the classical Otto cycle, a mixture of fuel and air is ignited by a spark plug. The timing of the spark heavily affects the combustion timing. The combustion then proceeds as a turbulent flame front through the combustion chamber. The Otto engines of today with modern after-treatment sys-

tems produce very small amounts of engine-out NO_x and soot. However, SI engines typically have poor efficiency at part load, increasing the fuel consumption.

CI Engines

In Compression Ignition (CI) engines, air (and possibly re-inducted exhausts) are compressed, following the Diesel cycle. The fuel is injected and combustion is initiated due to the high in-cylinder temperature. The emissions of NO_x and soot are typically higher than those of SI engines since parts of the combustion occurs in zones around the injected fuel spray. The efficiency, however, is also higher, yielding a lower fuel consumption and thereby less CO_2.

2.2 HCCI

This section outlines the development of the Homogeneous Charge Compression Ignition engine, the operating principle, and the need for closed-loop control.

HCCI Background

Early studies of HCCI were made on two-stroke engines and include [Onishi *et al.*, 1979; Ishibashi and Asai, 1979]. In the eighties, [Najt and Foster, 1983] showed HCCI operation in a four-stroke engine. During the nineties HCCI research increased, largely due to the possibility of decreased emissions. Publications from the late nineties include [Aoyama *et al.*, 1996; Christensen *et al.*, 1999]. This work has continued and the last ten years has seen much research aimed at making HCCI feasible for the market.

HCCI Operation

HCCI is characterized by auto-ignition of a homogeneous fuel-air mixture. There is no spark or injection event that triggers combustion. Instead, the auto-ignition is determined by the properties of the charge, the temperature, and the pressure [Chiang and Stefanopoulou, 2006; Bengtsson *et al.*, 2007]. HCCI has the advantage of a combustion without hot zones which reduces NO_x-emissions and since the charge is ho-

mogeneous no locally rich zones occur, reducing soot formation [Heywood, 1988]. The efficiency in part-load is fairly high which reduces fuel consumption and thereby CO_2-emissions.

A somewhat simplified HCCI engine cycle can be described by the following five stages where *(up)* and *(down)* indicate whether the piston is moving upwards or downwards. This partitioning of the engine cycle will be used in the model derivation in Chapter 4. Four of the stages are also illustrated in Figure 2.1, which also shows the opening of the inlet and exhaust valves.

1. Intake: The intake valve opens and a homogeneous mixture of fuel and air enters the cylinder *(down)*;

2. Compression: The intake valve closes and the in-cylinder charge is compressed *(up)*.

3. The charge auto-ignites;

4. Expansion: The pressure increase from the combustion forces the piston downwards and work is extracted *(down)*;

5. Exhaust: The exhaust valve opens and the residual gases leave the cylinder *(up)*.

Figure 2.2 shows the basic geometry of a cylinder. The movement of the piston is translated to rotation of the drive shaft. The rotation
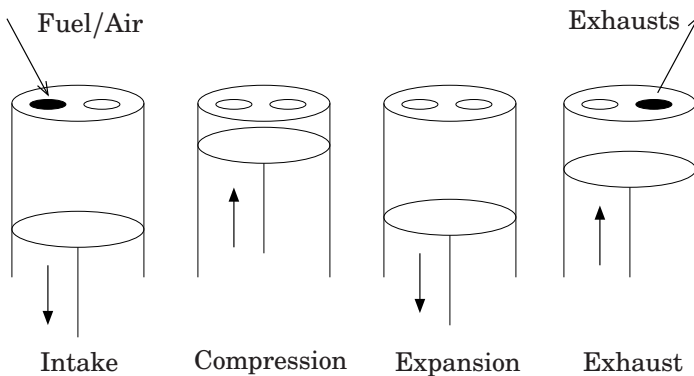
Figure 2.1   Principle of HCCI combustion. Black indicates an open valve.

15
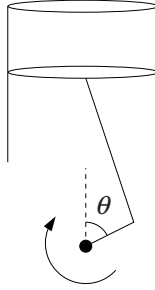
Figure 2.2   Basic geometry of a combustion engine cylinder showing the definition of the crank angle degree, θ.

is measured in Crank Angle Degrees (CAD), denoted θ. The top and bottom positions of the piston are denoted Top Dead Center (TDC) and Bottom Dead Center (BDC) respectively.

To achieve HCCI, a fairly high initial temperature is needed. One way of accomplishing such temperature is to re-induct the exhausts of the previous cycle. This can be done either by *trapping* where the exhaust valve is closed before the cylinder has been entirely scavenged [Shaver *et al.*, 2006b], or by introducing an additional opening of the exhaust valve, called *re-breathing* [Chiang *et al.*, 2007]. In this thesis, the increased initial temperature is achieved using an electric heater on the intake air. However, the presence of inert exhaust gases still affects the combustion. A long-route Exhaust Gas Recirculation (EGR) system can be used to dilute the charge. This increases the specific heat capacity of the charge, yielding a lower peak temperature.

HCCI Control

An inherent difficulty with HCCI lies in controlling the point of auto-ignition. As there is a wide range of factors that influence the combustion phasing, there are several possible control signals but also many possible disturbances that the control system must account for or be robust towards. Possible control signals that have been tried in experiments include [Bengtsson *et al.*, 2007] variable valve timing, intake temperature, the amount of residuals trapped in the cylinder, as well as mixing fuels with different octane number [Strandh *et al.*, 2004].

Figure 2.3 visualizes a possible categorization of control efforts for HCCI. The top level involves minimizing emissions, engine noise, and fuel consumption. The next level is combustion phasing control and the finally actuator control. For HCCI to be a viable choice for production vehicles, an additional control level is necessary as the driver must be able to give set-points in terms of, e.g., engine torque. The work in this thesis is focused on achieving robust, model-based, control of the combustion phasing. A few topics related to actuator control are discussed in Chapter 5.
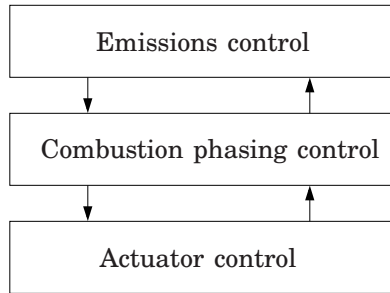
Figure 2.3   Possible categorization of HCCI control.

HCCI Modeling

Combustion engine modeling covers a wide range of model structures and levels of detail and complexity. Highly detailed Computational Fluid Dynamics (CFD) models are used to gain understanding of the physical process in different operating modes. This type of model is also suitable for design of the engine itself. Control-oriented models are typically characterized by lower complexity to enable control design and fast simulation. The models used for control design are often formulated on a cycle-to-cycle basis as this is natural for most of the considered control signals and well known, discrete-time, control design methods can be used. The two main categories are statistical models, obtained via system identification, and physical models, obtained from first principles and heuristic relationships. This thesis deals with models in the latter category. A review of previous work in this area is given in Section 4.1

2.3 Pressure Sensors

Throughout this work, it is assumed that in-cylinder pressure sensors are available. The measured pressure as a function of crank angle, $P(\theta)$, can be used to calculate relevant engine variables. A simplified rate of heat release can be calculated as

$$\frac{dQ}{d\theta} = \frac{\gamma}{\gamma - 1} P(\theta) \frac{dV}{d\theta} + \frac{1}{\gamma - 1} V(\theta) \frac{dP}{d\theta} \tag{2.1}$$

where $V(\theta)$ is the cylinder volume and γ is the specific heat ratio [Heywood, 1988]. From the heat release, the crank angle corresponding to a certain fraction of released energy, θ_x, can be calculated. It is defined by

$$x = \frac{Q(\theta_x)}{\max\limits_{\theta} Q(\theta)} \tag{2.2}$$

Fractions such as θ_{10}, θ_{50}, and θ_{90} are often used to characterize the combustion. The net Indicated Mean Effective Pressure (IMEP_n) can also be determined from the pressure trace

$$\text{IMEP}_n = \frac{1}{V_d} \int\limits_{\text{cycle}} P(\theta) dV \tag{2.3}$$

where V_d is the displacement volume. This produces a measure of the work output, normalized by the displacement volume.

Currently, pressure sensors are not implemented in production engines. It is likely that cost-effective and reliable sensors will be available in the future, making these control strategies feasible. Also, some research is aimed at removing the need for pressure sensors by using ion-current sensors in the combustion chamber [Strandh *et al.*, 2003] or knock sensors mounted on the engine block [Chauvin *et al.*, 2008].

3

Experimental Setup

Two different engines were used in this work. Data from an optical, single-cylinder, engine was used for validating the model presented in Chapter 4 while a six-cylinder metal engine was used for the control experiments in Chapters 6 and 7. Both engines were equipped with cylinder pressure sensors and operated using port fuel injection.

3.1 Optical Engine

The optical engine was a Scania heavy-duty diesel engine converted to single-cylinder operation. The engine was equipped with a quartz piston allowing measurements of the wall temperature to be made using thermographic phosphors. For further details on the measurement technique, see [Wilhelmsson *et al.*, 2005]. Table 3.1 contains geometric data and relevant valve timings for the engine. During the experiments, the engine was operated manually and only the injected fuel amount was varied in the experiments. The fuel used was iso-octane.

3.2 Metal Engine

The metal engine was a Volvo heavy-duty diesel engine. The engine and the control system was described in detail in [Karlsson, 2008] and is based on the system used in [Strandh, 2006; Bengtsson, 2004]. The

Table 3.1 Optical Engine Specifications

Displacement volume	1966 cm^3
Bore	127.5 mm
Stroke	154 mm
Connecting rod length	255 mm
Compression ratio	16:1
Exhaust valve open	34° BBDC
Exhaust valve close	6° BTDC
Inlet valve open	2° BTDC
Inlet valve close	29° ABDC

Table 3.2 Metal Engine Specifications

Displacement volume	2000 cm^3
Bore	131 mm
Stroke	150 mm
Connecting rod length	260 mm
Compression ratio	18.5:1
Exhaust valve open	101° ATDC
Exhaust valve close	381° ATDC
Inlet valve open	340° ATDC
Inlet valve close	variable

engine specifications are presented in Table 3.2. The fuel used was ethanol.

The control system was run on a PC-computer running Linux. Controllers were designed in MATLAB/Simulink and converted to C-code using Real-Time Workshop [Mathworks, 2004]. A graphical user interface allowed enabling and disabling controllers as well as manual control of all variables. The computer had a 2.4 GHz Intel Pentium 4 processor. The experiments were performed at a nominal engine speed of 1200

rpm, yielding a sample time of 0.1 seconds per cycle. A wide selection of possible control signals were available. The control signals used in this work were the crank angle of inlet valve closing (θ_{IVC}) and the intake temperature (T_{in}). In the robustness investigation in Chapter 7 the possibility of varying the engine speed, the amount of injected fuel, and the amount of recycled exhausts were utilized. The engine was equipped with a long-route Exhaust Gas Recirculation (EGR) system.

4

Modeling

This chapter describes a cycle-resolved model of HCCI incorporating cylinder wall temperature dynamics. The model is based on the model in [Shaver *et al.*, 2006b], it uses the same basic formulation and assumptions with the addition of cylinder wall temperature dynamics and a few modifications. The considered outputs were the Indicated Mean Effective Pressure (IMEP_n) and the crank angle where 50% of the total heat has been released (θ_{50}). The motivation for this choice is that IMEP_n relates to the work output of the engine and that θ_{50} has been shown to be a robust indicator of combustion phasing [Bengtsson, 2004]. The model structure is fairly modular in the choice of control signals. The model was validated using data from step changes in the amount of fuel. During the control experiments presented in Chapters 6 and 7 the crank angle of inlet valve closing, θ_{IVC}, and the intake temperature, T_{in}, were used as control signals. The model also describes the effects of varying the amount of recycled exhaust gases and varying the exhaust valve opening.

4.1 Motivation

To facilitate model-based control design, both statistical and physical models have been considered [Bengtsson *et al.*, 2007]. A drawback with statistical models is that the models, and the resulting controllers, are difficult to migrate to a different engine or operating point, whereas physical models typically require only re-calibration of physical param-

eters. Calibration of parameters is not always a trivial task, but it may require less calibration data to yield a model which is valid in a fairly large operating range. Another benefit of physical models is that they offer some understanding of the engine behaviour. Most control-oriented physical models of HCCI are either formulated in continuous time or on a cycle-to-cycle basis [Bengtsson *et al.*, 2007]. The models in the former category allow for a natural formulation, e.g., of flow phenomena, while those in the latter take a form suitable for cycle-to-cycle control design. Continuous-time models of HCCI include [Shaver *et al.*, 2006a; Bengtsson *et al.*, 2004].

Heat transfer between the in-cylinder charge and the cylinder walls is an important effect for explaining HCCI cycle-to-cycle behaviour under certain operating conditions [Blom *et al.*, 2008]. Also, experimental data show considerable variations in wall temperature with varying operating conditions [Wilhelmsson *et al.*, 2005]. However, many modeling approaches for control only consider heat transfer from the gases to the walls during combustion and assume a constant cylinder wall temperature [Bengtsson *et al.*, 2007].

Continuous-time models including cylinder wall temperature models were presented in [Roelle *et al.*, 2006; Blom *et al.*, 2008]. The latter synthesized an LQ controller using a cycle-resolved statistical version of the model and presented experimental results. A GT-power® based engine model augmented with a heat transfer model was used in a simulation study in [Chang *et al.*, 2007]. A more detailed study of the cylinder wall temperature was done in [Rakopoulos *et al.*, 2004], where Fourier analysis was applied to capture spatial variations. The resulting model formulation is, however, less suitable for control design than the low-complexity model presented in this thesis. An experimental study of the cylinder wall temperature variations within a single engine cycle was presented in [Särner *et al.*, 2005].

Recent examples of cycle-resolved models of HCCI for control design include [Chiang *et al.*, 2007; Shaver *et al.*, 2006b; Rausen *et al.*, 2004], where [Shaver *et al.*, 2006b] also presented experimental results of closed-loop control. The models contain a cycle-to-cycle coupling through the residual gas temperature, also included in the model that will be derived here. However, when there is only little residuals present in the cylinder it is more physically reasonable to let the cylinder wall temperature link the cycles. A cycle-resolved model including

heat transfer effects was presented in [Canova *et al.*, 2005] where the wall surface temperature was determined by averaging the gas and coolant temperatures. A cycle-resolved model tracking species concentration was presented in [Ravi *et al.*, 2006].

4.2 Cylinder Wall Temperature Dynamics
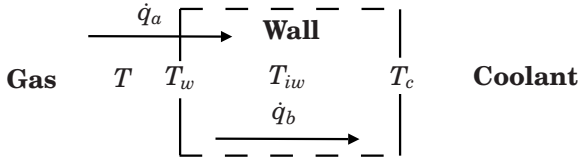
Figure 4.1   Principle of the cylinder wall model.

The cylinder wall was modeled as a single mass with a slowly varying outer surface temperature T_c, a convective flow $\dot{q}_a$ between the in-cylinder gases and the cylinder wall, and a conductive flow $\dot{q}_b$ through the wall, see Figure 4.1.

The first law of thermodynamics applied to the gas when no work is performed yields

$$\dot{T} = -\frac{\dot{q}_a}{mC_v} \tag{4.1}$$

where T, m, and C_v are the temperature, mass, and specific heat of the gas. The Newton law

$$\dot{q}_a = h_c A_c (T - T_w) \tag{4.2}$$

was applied, where h_c is the convection coefficient, A_c is the wall surface area and T_w is the wall surface temperature. The convection coefficient is often modeled using the following expression [Bengtsson *et al.*, 2007],

$$h_c = 3.26 B^{-0.2} P^{0.8} T^{-0.55} (2.28 S_p)^{0.8} \tag{4.3}$$

where B is the cylinder bore, P is the in-cylinder pressure, T is the gas temperature, and S_p is the mean piston speed [Woschni, 1967].

The time derivative of the inner wall temperature, T_{iw}, is given by

$$\dot{T}_{iw} = \frac{\dot{q}_a - \dot{q}_b}{m_c C_p} \tag{4.4}$$

where C_p is the specific heat of the cylinder wall, and m_c is the cylinder wall mass. The conductive flow is given by

$$\dot{q}_b = \frac{(T_w - T_c)k_c A_c}{L_c} \tag{4.5}$$

where k_c is the conduction coefficient and L_c is the wall thickness. Assuming that the steady-state temperature condition

$$T_{iw} = \frac{T_w + T_c}{2} \tag{4.6}$$

holds, the temperature equations may be written as

$$\dot{\mathcal{T}} = A_{ht}\mathcal{T} + B_{ht}T_c, \tag{4.7}$$

where

$$A_{ht} = \begin{pmatrix} -\dfrac{h_c A_c}{m C_v} & \dfrac{h_c A_c}{m C_v} \\ 2\dfrac{h_c A_c}{m_c C_p} & -2\dfrac{h_c A_c + k_c A_c/L_c}{m_c C_p} \end{pmatrix},$$

$$B_{ht} = \begin{pmatrix} 0 \\ 2\dfrac{k_c A_c}{L_c m_c C_p} \end{pmatrix}, \quad \mathcal{T} = \begin{pmatrix} T \\ T_w \end{pmatrix} \tag{4.8}$$

Similar assumptions were made in [Blom *et al.*, 2008; Roelle *et al.*, 2006]. The resulting model was used in a continuous-time formulation in [Blom *et al.*, 2008] while [Roelle *et al.*, 2006] updated the wall temperature once per cycle combined with continuous-time gas temperature dynamics.

Since T_c is assumed to be slowly varying, it can be assumed constant over a short time t_i. The temperature state at t_i, given an initial state $\mathcal{T}(0)$, can then be computed as

$$\mathcal{T}(t_i) = \Phi_i \mathcal{T}(0) + \Gamma_i T_c \tag{4.9}$$

where

$$\Phi_i = e^{A_{ht}t_i}, \quad \Gamma_i = \int_0^{t_i} e^{A_{ht}(t_i-\tau)} B_{ht} d\tau \tag{4.10}$$

Equation (4.9) was used to update the gas temperature and the wall temperature after mixing, after combustion, and after expansion. This approach allows tracking of the temperature dynamics of gas and cylinder wall during the cycle while keeping the complexity low. Since the integration time t_i had to be adapted to each instant and some of the parameters depend on the in-cylinder state, three sets of matrices $\{\Phi_i, \Gamma_i\}$, $i = 1, 3, 5$ were used. With the notation in Section 2.2 $i = 1$ corresponded to mixing, $i = 3$ corresponded to combustion, and $i = 5$ corresponded to expansion. The cylinder wall temperature was assumed constant between the heat transfer events.

4.3 Temperature Trace

In this section the evolution of the gas temperature, the pressure, and the wall temperature during an engine stroke is presented. Indices in parentheses denote cycle number while subscripts denote stages within the cycle. For example, $T_1(k)$ denotes the gas temperature after intake in cycle k. The subscript '+' is added to the temperatures after (4.9) has been applied to model heat transfer, e.g. $T_{1+}(k)$. The crank angle is denoted θ. The crank angle at inlet valve closing and the crank angle at auto-ignition in cycle k are denoted $\theta_{\text{IVC}}(k)$ and $\theta_{\text{ign}}(k)$ respectively.

The cylinder volume corresponding to a certain crank angle can be determined using [Heywood, 1988]

$$V(\theta) = V_c + \frac{V_d}{2}\left(R_v + 1 - \cos(\theta) - \sqrt{R_v^2 - \sin^2(\theta)}\right) \tag{4.11}$$

where V_d is the displacement volume, V_c is the clearance volume, and R_v is the ratio between the connecting rod length and the crank radius.

The chemical reaction describing complete, stoichiometric, combustion of a hydrocarbon C_xH_y in air can be written [Heywood, 1988]

$$C_xH_y + \left(x + \frac{y}{4}\right)O_2 + 3.778\left(x + \frac{y}{4}\right)N_2 \rightarrow$$
$$xCO_2 + \frac{y}{2}H_2O + 3.778\left(x + \frac{y}{4}\right)N_2 \tag{4.12}$$
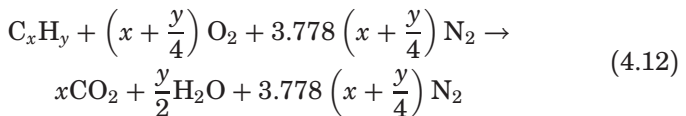
Calibration data for the model was obtained using iso-octane, C_8H_{18}, while the control experiments were done using ethanol, C_2H_5OH. The extra oxygen in ethanol modifies the reaction formula in (4.12) somewhat since less air is needed.

Throughout the cycle, isentropic expansion and compression was assumed. The following definitions can be found, e.g., in [Heywood, 1988].

DEFINITION 4.1
The temperature T_B and pressure P_B after isentropic compression or expansion from volume V_A to a volume V_B with initial temperature and pressure T_A and P_A are given by

$$T_B = T_A \left(\frac{V_A}{V_B} \right)^{\gamma-1}, \quad P_B = P_A \left(\frac{V_A}{V_B} \right)^{\gamma} \tag{4.13}$$

where γ is the specific heat ratio. $\quad\square$

DEFINITION 4.2
The temperature T_B after isentropic compression or expansion from a pressure P_A to a pressure P_B is given by

$$T_B = T_A \left(\frac{P_B}{P_A} \right)^{(\gamma-1)/\gamma} \tag{4.14}$$

$\square$

Intake/Mixing The gas temperature at the start of cycle k, $T_1(k)$, was modeled as the weighted average of the intake temperature and the temperature of the trapped residuals, cf. [Shaver *et al.*, 2006b];

$$T_1(k) = \frac{C_{v,\text{in}} T_{\text{in}}(k) + C_{v,\text{EGR}} \chi \alpha T_{5+}(k-1)}{C_{v,\text{in}} + \alpha C_{v,\text{EGR}}}, \tag{4.15}$$

where $C_{v,\text{in}}$ and $C_{v,\text{EGR}}$ are the specific heats of the fresh reactants and the residual gases respectively, given by the weighted average of the heat capacities of the reactants on each side of (4.12). The final gas

temperature of cycle $k-1$ is denoted $T_{5+}(k-1)$ and the parameter $\chi \in [0,1]$ models cooling of the residuals since the previous cycle. The molar ratio between trapped residuals and inducted gases is denoted α and given by

$$\alpha = \frac{n_p}{n_a + n_f}, \tag{4.16}$$

where n_p, n_a, and n_f are the molar amounts of products, air, and fuel respectively. If there is no trapping, α is (or is close to) zero. The amount of long-route, cooled, recycled exhausts instead affects $C_{v,\text{in}}$. An additional parameter could be used to describe the molar ratio between cooled exhausts and fresh charge. The initial wall temperature of cycle k was set equal to the final wall temperature of cycle $k-1$;

$$T_{w1}(k) = T_{w5+}(k-1) \tag{4.17}$$

Eq. (4.9) with $i=1$ was applied to yield new temperatures $T_{1+}(k)$ and $T_{w1+}(k)$;

$$\begin{pmatrix} T_{1+}(k) \\ T_{w1+}(k) \end{pmatrix} = \Phi_1 \begin{pmatrix} T_1(k) \\ T_{w1}(k) \end{pmatrix} + \Gamma_1 T_c \tag{4.18}$$

Compression   Isentropic compression from the volume at inlet valve closing, $V_1(k)$, to the volume at auto-ignition, $V_2(k)$, was assumed, yielding temperature $T_2(k)$ and pressure $P_2(k)$.

$$T_2(k) = T_{1+}(k) \left(\frac{V_1(k)}{V_2(k)} \right)^{\gamma - 1}, \quad P_2(k) = P_{\text{in}} \left(\frac{V_1(k)}{V_2(k)} \right)^{\gamma} \tag{4.19}$$

where P_{in} is the intake pressure.

Auto-Ignition   Modeling of the crank angle of auto-ignition, θ_{ign}, is described in Section 4.4.

Combustion   Assuming complete, isochoric combustion without heat losses to the cylinder walls, the mean gas temperature after combustion is [Heywood, 1988]

$$T_3(k) = T_2(k) + \frac{m_f}{m} \frac{Q_{\text{LHV}}}{C_v}, \tag{4.20}$$

where Q_{LHV} is the lower heating value of the fuel and m_f is the fuel mass. The total gas mass can be decomposed as

$$m = m_a + m_f + m_p, \tag{4.21}$$

where m_p is the mass of the residuals from the previous cycle. Using the definition of equivalence ratio

$$\phi = (m_f/m_a)/(m_f/m_a)_s, \tag{4.22}$$

where $(m_f/m_a)_s$ is the stoichiometric fuel-air ratio and m_a is the air mass, (4.16), and (4.21) the ratio m_f/m in (4.20) can be estimated as

$$\frac{m_f}{m} = \frac{1}{\left(\phi^{-1}(m_a/m_f)_s + 1\right)(1 + f_\alpha(\phi))}, \tag{4.23}$$

where

$$f_\alpha(\phi) = \frac{\alpha M_p}{\phi^{-1}(m_a/m_f)_s + 1}\left(\frac{\phi^{-1}(m_a/m_f)_s}{M_a} + \frac{1}{M_f}\right) \tag{4.24}$$

with M_p, M_a, and M_f denoting the molar masses of the products, air, and fuel respectively. However, the variation in $f_\alpha(\phi)$ for the values of ϕ investigated was less than one percent. For simplicity, the approximation

$$\frac{m_p}{m_a + m_f} \approx \alpha \tag{4.25}$$

was used, replacing $f_\alpha(\phi)$ with α in (4.23) yielding an error of less than one percent in the mass ratio estimate. This yields the following expression for $T_3(k)$.

$$T_3(k) = T_2(k) + \frac{Q_{\text{LHV}}}{(1 + \alpha)(\phi^{-1}(m_a/m_f)_s + 1)C_v} \tag{4.26}$$

Eq. (4.9) was then applied with $i = 3$ and $T_{w3}(k) = T_{w1+}(k)$ to find new temperatures $T_{3+}(k)$, $T_{w3+}(k)$.

$$\begin{pmatrix} T_{3+}(k) \\ T_{w3+}(k) \end{pmatrix} = \Phi_3 \begin{pmatrix} T_3(k) \\ T_{w3}(k) \end{pmatrix} + \Gamma_3 T_c \tag{4.27}$$

The pressure after combustion is then

$$P_3(k) = \frac{T_{3+}(k)}{T_2(k)} P_2(k) \tag{4.28}$$

Expansion The gas temperature and pressure after expansion, $T_4(k)$ and $P_4(k)$, were calculated assuming adiabatic expansion from $V_2(k)$ to the volume at exhaust valve opening, $V_4(k)$.

$$T_4(k) = T_{3+}(k) \left(\frac{V_2(k)}{V_4(k)} \right)^{\gamma-1}, \quad P_4(k) = P_3(k) \left(\frac{V_2(k)}{V_4(k)} \right)^{\gamma} \tag{4.29}$$

At exhaust valve opening, isentropic expansion from the in-cylinder pressure to atmospheric pressure was assumed, yielding temperature $T_5(k)$.

$$T_5(k) = T_4(k) \left(\frac{P_{\text{in}}}{P_4(k)} \right)^{(\gamma-1)/\gamma} \tag{4.30}$$

Finally, Eq. (4.9) was applied with $i = 5$ and $T_{w5}(k) = T_{w3+}(k)$ to obtain the final gas temperature $T_{5+}(k)$ and the final wall temperature $T_{w5+}(k)$.

$$\begin{pmatrix} T_{5+}(k) \\ T_{w5+}(k) \end{pmatrix} = \Phi_5 \begin{pmatrix} T_5(k) \\ T_{w5}(k) \end{pmatrix} + \Gamma_5 T_c \tag{4.31}$$

4.4 Prediction of Auto-ignition

Since control of the combustion phasing is central to successful implementation of HCCI, several models for the auto-ignition in HCCI have been suggested. The physics-based approaches include knock integrals [Hillion *et al.*, 2008; Shahbakhti and Koch, 2007] and Arrhenius integrals in varying forms [Shaver *et al.*, 2006b; Chiang and Stefanopoulou, 2006]. Formulations aimed at control design include simplifying the Arrhenius integral [Shaver *et al.*, 2006b] as well as linear approximations [Chiang and Stefanopoulou, 2006].

The Arrhenius Integral

The onset of combustion is triggered by the formation of a critical amount of radicals (molecules with an unpaired electron) from stable species. The rate of formation of radicals, $R\cdot$, given on a crank angle basis, is given by

$$\frac{d[R\cdot]}{d\theta} = \kappa P^n(\theta) \exp\left(-\frac{E_a}{RT(\theta)} \right) [F]^a(\theta) [O_2]^b(\theta) \tag{4.32}$$

where κ is a scaling factor, T and P are the gas charge temperature and pressure respectively, R is the gas constant, E_a is the activation energy for the radical generation, and n, a, b are sensitivity measures towards pressure and concentrations of fuel and oxygen respectively [Chiang and Stefanopoulou, 2006]. The concentrations of fuel and oxygen are denoted [F] and [O]. By neglecting the small amount of radicals at the intake, i.e., setting $[R\cdot](\theta_{\mathrm{IVC}}) = 0$ the critical amount of radicals needed to initiate combustion, $[R\cdot]_c$, can be computed as

$$[R\cdot]_c = \int_{\theta_{\mathrm{IVC}}}^{\theta_{\mathrm{ign}}} \frac{d[R\cdot]}{d\theta} d\theta \qquad (4.33)$$

A sensitivity analysis presented in [Chiang and Stefanopoulou, 2006] suggested that the dependence on species concentration can be neglected, yielding the following alternative expression.

$$1 = \int_{\theta_{\mathrm{IVC}}}^{\theta_{\mathrm{ign}}} A_a P^n(\theta) \exp\left(-\frac{E_a}{RT(\theta)}\right) d\theta \qquad (4.34)$$

where A_a is a scaling factor and n is the reaction's sensitivity to pressure. Assuming isentropic compression the condition can be rewritten using the notation in Section 4.3 as

$$\int_{\theta_{\mathrm{IVC}}(k)}^{\theta_{\mathrm{ign}}(k)} f_k(\theta) d\theta = 1 \qquad (4.35)$$

where

$$f_k(\theta) = A_a P_{\mathrm{in}}^n \mathcal{V}_k^{\gamma n}(\theta) \exp\left(-\frac{E_a \mathcal{V}_k^{1-\gamma}(\theta)}{RT_{1+}(k)}\right) \qquad (4.36)$$

and $\mathcal{V}_k(\theta) = V_1(k)/V(\theta)$.

Simplifications

To obtain an explicit expression for θ_{ign} from an Arrhenius integral, an approach similar to that in [Shaver *et al.*, 2006b] can be taken. The integrand was approximated with its maximum value, which is attained at Top Dead Center (TDC). The corresponding crank angle degree (CAD) was denoted θ_{TDC}, so that $f_k(\theta) = f_k(\theta_{\mathrm{TDC}})$. The lower

integration limit was then shifted from θ_{IVC} to θ_{TDC} and the resulting integral equation was solved for $\theta_{\mathrm{ign}}(k)$;

$$\theta_{\mathrm{ign}}(k) = \Delta\theta_A + \frac{1}{f_k(\theta_{\mathrm{TDC}})} \tag{4.37}$$

where $\Delta\theta_A$ is an offset in CAD.

Another simplifying approach to prediction of auto-ignition was presented in [Chiang *et al.*, 2007], where a linear approximation of the dependence on the temperature at inlet valve closing was used.

$$\theta_{\mathrm{ign}}(k) = g_0(m_f) + g_1(m_f)T_{1+}(k) \tag{4.38}$$

where g_0 and g_1 are functions of the amount of injected fuel. This approach does not capture the dependence on the current value of θ_{IVC}.

4.5 Model Outputs

The model requires two variables to fully describe the state. The initial state selection was the resulting gas temperature and wall temperature of the cycle, $T_{5+}(k)$ and $T_{w5+}(k)$. The studied outputs were the crank angle of 50% burned, θ_{50}, and the indicated mean effective pressure, IMEP_n.

The combustion duration is a function of the charge temperature, composition, and θ_{ign} [Chiang and Stefanopoulou, 2006]. Around an operating point the combustion duration was assumed constant, yielding the following expression for θ_{50}, where $\Delta\theta$ is an offset in crank angle degrees.

$$\theta_{50}(k) = \theta_{\mathrm{ign}}(k) + \Delta\theta \tag{4.39}$$

IMEP_n was calculated from the gas temperatures [Heywood, 1988];

$$\mathrm{IMEP}_n(k) = \frac{mC_v}{V_d}\left(T_{1+}(k) - T_2(k) + T_{3+}(k) - T_4(k)\right) \tag{4.40}$$

The resulting model takes the form

$$x(k+1) = \mathbf{F}(x(k), u(k)) \tag{4.41a}$$
$$y(k) = \mathbf{G}(x(k), u(k)) \tag{4.41b}$$

where

$$x(k) = \begin{pmatrix} T_{5+}(k) \\ T_{w5+}(k) \end{pmatrix}, \quad y(k) = \begin{pmatrix} \text{IMEP}_n(k) \\ \theta_{50}(k) \end{pmatrix} \qquad (4.42)$$

and $u(k)$ contains the input variables, such as ϕ, T_{in}, and θ_{IVC}.

4.6 Calibration

The model was calibrated using measurement data from the optical engine described in Section 3.1. Data from a positive and a negative step change in the amount of fuel was available for calibration and validation.

Calibration of all Heat Transfer Parameters

The model was implemented in the Modelica language and then translated into AMPL code using the Optimica Compiler [Åkesson, 2007]. This allowed the parameter calibration process to be cast as an optimization problem minimizing the error between the model output and the measured output while respecting constraints on the parameter values. Only parameters connected to the heat transfer equations were optimized initially. A stationary operating point was used for the calibration and the model was then validated dynamically during step changes in the equivalence ratio. Calibration of the prediction of autoignition was done once the temperature trace had been determined.

Due to the structure of the matrices in (4.8) the parameters can be lumped into the following products; $(h_c A_c)_i$, $k_c A_c / L_c$, $1/m C_v$, and $1/m_c C_p$ where $i = 1, 3, 5$. The optimization parameters is then a vector p containing these six products and the integration times t_1, t_3, and t_5, as well as initial values, x_0, for the states. The optimization problem

can be written as

$$\underset{p,\,x_0}{\text{minimize}} \left(\text{IMEP}_n^m(k) - \text{IMEP}_n(k)\right)^2 + \left(T_w^m(k) - T_w(k)\right)^2$$

$$\begin{aligned}
\text{subject to} \qquad & \\
x(k+1) \;&=\; \mathbf{F}\left(x(k), u(k)\right) \\
y(k) \;&=\; \mathbf{G}\left(x(k), u(k)\right) \\
p \;&\in\; \mathcal{P} \\
x(k) \;&=\; x_0
\end{aligned} \tag{4.43}$$

where the superscript $'m'$ denotes measured values, $\mathcal{P}$ specifies the allowed parameter values, and the last constraint guarantees that the model is in steady state.

Calibration Results

Figure 4.2 shows the model outputs and the wall temperature during a positive step in the equivalence ratio from approximately $\phi = 0.12$ to approximately $\phi = 0.27$. The model captures the qualitative behaviour of all three variables. Figure 4.3 shows the model outputs and the wall temperature during a negative step in equivalence ratio from approximately $\phi = 0.27$ to approximately $\phi = 0.17$. Only parameters related to the prediction of θ_{50} were altered from the previous step response. The model somewhat overestimates the wall temperature and IMEP_n at the lower load.

It should be noted that the measurement of the equivalence ratio is a potential source of errors, as a sample of ϕ was obtained approximately every 20 engine cycles, which means that some transients in the model outputs may be due to unmeasured variations in equivalence ratio.

Calibration of Integration Times

The elements of the matrices in (4.8) all have a physical interpretation. This can be utilized to reduce the number of parameters that need to be adapted to a certain engine. In this section the possibility of using physics-based estimates of the parameters is discussed. The only remaining tuning parameters are then the integration times t_1, t_3, t_5, and the initial temperature state.
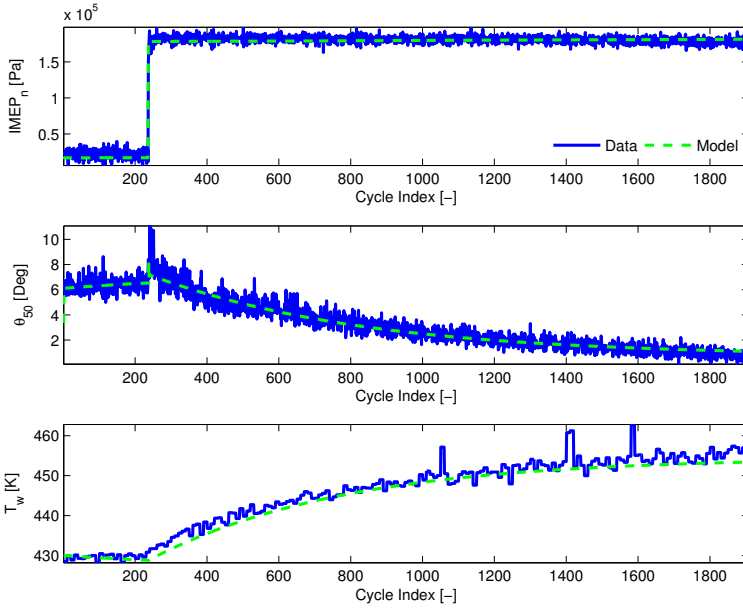
Figure 4.2 IMEP$_n$, θ_{50}, and T_w measured and model output during a positive step in equivalence ratio.

Physics-based Parameter Estimates The heating values of the charge and the wall, as well as the conduction coefficient of the wall material can be found in, or calculated from, tables [Heywood, 1988].

The gas mass can be estimated using the ideal gas law and knowledge of the thermodynamic state at inlet valve closing. The wall mass and thickness can be estimated using geometric data on the engine. The wall area, A_c is a function of the crank angle and can be expressed as a function of the volume $V(\theta)$ as follows

$$A_c(\theta) = \frac{\pi B^2}{2} + 4\frac{V(\theta)}{B} \tag{4.44}$$

The average area during each heat transfer instant could therefore be used.

As mentioned in Section 4.2, the convection coefficient, h_c, is often

35
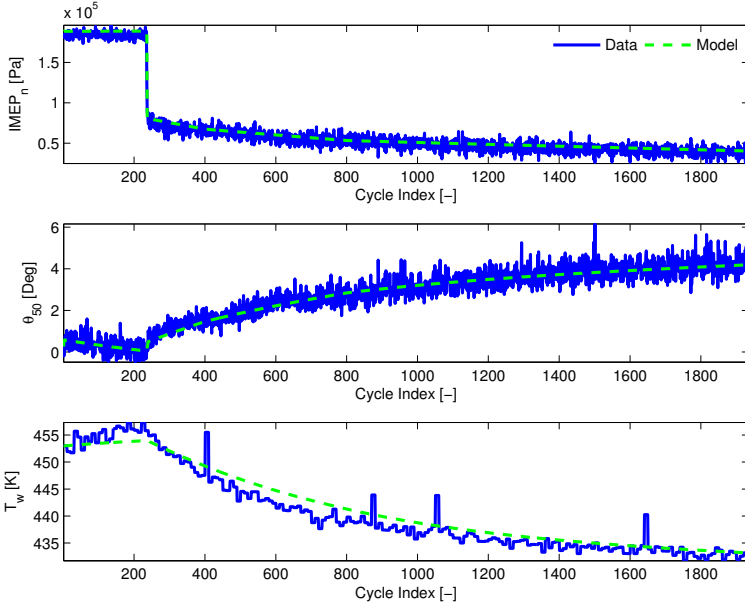
Figure 4.3   IMEP$_n$, θ_{50}, and T_w measured and model output during a negative step in equivalence ratio.

modeled using the Woschni expression in (4.3). It is suggested in [Soyhan *et al.*, 2009] that a more suitable choice for HCCI conditions is the Hohenberg expression [Hohenberg, 1979]

$$h_c = \alpha_s L^{-0.2} P^{0.8} T^{-0.73} v_{\text{tuned}}^{0.8} \qquad (4.45)$$

where α_s is a scaling factor, L is the instantaneous chamber height, and v_{tuned} is a function of the mean piston speed, volume, temperature, and pressure. A modified version of the Woschni expression was also presented in [Chang *et al.*, 2004]. Regardless of the expression used, average values of h_c can be determined for a specified crank angle interval.

Optimization Method   The remaining parameters are the integration times, t_1, t_3, and t_5. For open-loop simulation, the initial state x_0

also needs to be selected. If a pre-determined method is used for pre-diction of auto-ignition, such as an Arrhenius integral with parameters adapted to the specific fuel, the optimization criterion is

$$\underset{x_0,t_1,t_3,t_5}{\text{minimize}} \sum_{k=k_0}^{k_N} \tilde{\theta}_{50}^2(k) + \delta_1(\text{IMEP}_n^m(k) - \text{IMEP}_n(k))^2$$

$$\text{subject to}$$
$$\begin{aligned} x(k+1) &= \mathbf{F}(x(k),u(k)) \\ y(k) &= \mathbf{G}(x(k),u(k)) \\ x(k) &= x_0 \end{aligned} \tag{4.46}$$

where $\delta_1 \geq 0$ is a weight, $\tilde{\theta}_{50}(k) = \theta_{50}^m(k) - \theta_{50}(k)$, and the last condition requires that the model is in steady state if only steady state measurement data is used for the calibration. To allow for some variation in the wall temperature, a regularized formulation can be used.

$$\underset{x_0,t_1,t_3,t_5}{\text{minimize}} \sum_{k=k_0}^{k_N} \tilde{\theta}_{50}^2(k) + \delta_1(\text{IMEP}_n^m(k) - \text{IMEP}_n(k))^2 + \delta_2(\Delta x(k))^2$$

$$\text{subject to}$$
$$\begin{aligned} x(k+1) &= \mathbf{F}(x(k),u(k)) \\ y(k) &= \mathbf{G}(x(k),u(k)) \\ x(k_0) &= x_0 \end{aligned}$$

$$\tag{4.47}$$

where $\Delta x(k) = x(k) - x(k-1)$ and $\delta_2 \geq 0$ is a weight.

4.7 Discussion

The cylinder wall temperature is a good candidate for explaining the slower modes of HCCI dynamics observed in experimental data. The model states are the mean gas temperature and the mean wall temperature after the exhaust valve has opened. These states are not measurable on an actual engine but, as is shown in Chapter 5, the model
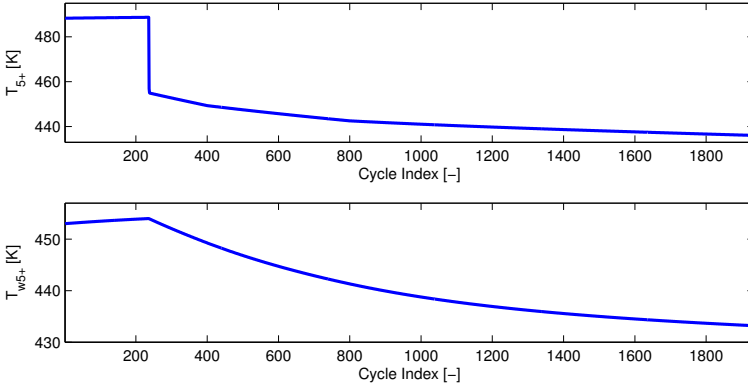
Figure 4.4   The simulated states, T_{5+} and T_{w5+} during the negative step in equivalence ratio.

formulation allows using IMEP_n and θ_{50} as states, enabling state feedback.

State Evolution

In order to see the interaction between gas temperature and wall temperature, the states, obtained from open-loop simulation, during the negative step in ϕ are shown in Figure 4.4. There is an immediate decrease in gas temperature in response to the reduction in injected fuel. However, the dependence on the wall temperature is evident after this initial transient.

Prediction of Auto-Ignition

Equation (4.38) assumes a linear relation between the temperature at inlet valve closing and θ_{50}, as suggested in [Chiang *et al.*, 2007]. Since the prediction of auto-ignition was initially left out of the calibration, the applicability of this assumption can be evaluated by comparing the vector of $T_{1+}(k)$ with the measured $\theta_{50}(k)$. Figure 4.5 shows a scatter plot of the two for cycle indices greater than 400 during the steps in ϕ shown in Figures 4.2 and 4.3. The assumption of a linear dependence between $\theta_{50}(k)$ and $T_{1+}(k)$ seems reasonable in this case. However, while the Arrhenius-based method in (4.37) does increase the
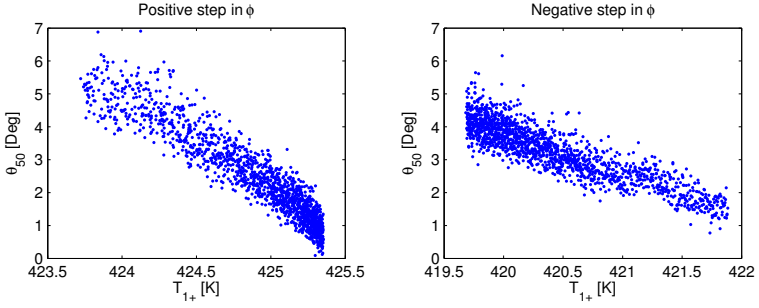
Figure 4.5 Scatter plot of θ_{50} and T_{1+} for cycle indexes greater than 400 during the steps in ϕ shown in Figures 4.2 and 4.3.

model complexity somewhat, it offers an explicit dependence on θ_{IVC} and the intake pressure. This dependence is of importance, e.g., when the intake valve closing is used as a control signal.

5

Control

This chapter discusses control design based on the model in Chapter 4. First, the temperature state is replaced by IMEP_n and θ_{50}, so that state feedback is possible. The considered control signals are then discussed and two approaches for handling initially unmodeled dynamics in an actuator are presented. The chapter concludes with the basics of Model Predictive Control.

5.1 State Selection

The model requires two variables to fully describe the temperature state. In the original model formulation, the states were the final gas temperature, $T_{5+}(k)$, and the final wall temperature, $T_{w5+}(k)$. Due to the simplified auto-ignition model it is possible to uniquely determine the states from the current output measurement. Using (4.9), (4.36), (4.37), (4.26), (4.39), (4.40), and the assumption of isentropic compression and expansion, the temperature state can be uniquely determined from the outputs.

$$T_{1+}(k) = \frac{E_a \mathcal{V}_k^{1-\gamma}(\theta_{\text{TDC}})}{R \ln \left(A_a P_{\text{in}}^n \mathcal{V}_k^{\gamma n}(\theta_{\text{TDC}}) \theta_m(k) \right)} \tag{5.1}$$

where $\theta_m(k) = \theta_{50}(k) - \Delta\theta_A - \Delta\theta$. The corresponding wall temperature can then be calculated as

$$T_{w1+}(k) = \frac{\text{IMEP}_n(k) - (mC_v/V_d)\left(c_1 T_{1+}(k) + c_2 c_3\right)}{c_3(mC_v/V_d)\Phi_{3[1,2]}}, \tag{5.2}$$

where

$$c_1 = 1 - \left(\frac{V_1}{V_2}\right)^{\gamma-1} + c_3 \Phi_{3[1,1]} \left(\frac{V_1}{V_2}\right)^{\gamma-1} \qquad (5.3a)$$

$$c_2 = \frac{\Phi_{3[1,1]} Q_{\mathrm{LHV}}}{(1+\alpha)\left(\phi^{-1}\left(\frac{m_a}{m_f}\right)_s + 1\right) C_v} + \Gamma_{3[1,1]} T_c \qquad (5.3b)$$

$$c_3 = 1 - \left(\frac{V_2(k)}{V_4(k)}\right)^{\gamma-1} \qquad (5.3c)$$

and $\Phi_{3[x,y]}$ indicates element (x,y) of Φ_3. By going through the cycle the final temperatures are obtained and can be propagated to cycle $k+1$. The model then takes the following form.

$$y(k+1) = \mathbf{F}(y(k), u(k)) \qquad (5.4)$$

where

$$y(k) = \begin{pmatrix} \mathrm{IMEP}_n(k) \\ \theta_{50}(k) \end{pmatrix}, \quad u(k) = \begin{pmatrix} \theta_{\mathrm{IVC}}(k) \\ T_{\mathrm{in}}(k) \end{pmatrix} \qquad (5.5)$$

The function $\mathbf{F}(y(k), u(k))$ is parametrized by the amount of injected fuel, the amount of recycled exhaust gases, the intake pressure, etc.

5.2 Linearization

Due to the complexity introduced by the heat transfer events, the resulting model equations are not easily tractable by hand. The symbolic toolbox in MATLAB was used to obtain linearizations according to

$$y(k+1) = Ay(k) + Bu(k) \qquad (5.6)$$

where

$$A = \frac{\partial \mathbf{F}(y(k), u(k))}{\partial y(k)}(y^0, u^0), \quad B = \frac{\partial \mathbf{F}(y(k), u(k))}{\partial u(k)}(y^0, u^0) \qquad (5.7)$$

where (y^0, u^0) is a stationary operating point. Figure 5.1 shows the simulated response from the nonlinear model and that of the linearized

model. The fit between the two is rapidly deteriorating with increasing distance to the linearization point. Inspired by this observation a suitable approach may be to use a piece-wise linear (sometimes referred to as linear parameter-varying) approximation of the nonlinear model containing multiple linearizations, replacing (5.6) with

$$y(k+1) = A_j y(k) + B_j u(k), \quad j = g(y(k)) \tag{5.8}$$

where $g(y(k))$ maps the current output measurement to the corresponding linearization. Using three linearizations, and switching based on the θ_{50} measurement, the L_2-error in IMEP$_n$ and θ_{50} was decreased by 26% and 10% respectively during the trajectory shown in Figure 5.1. Control simulations based on this model will be evaluated in Section 6.2.
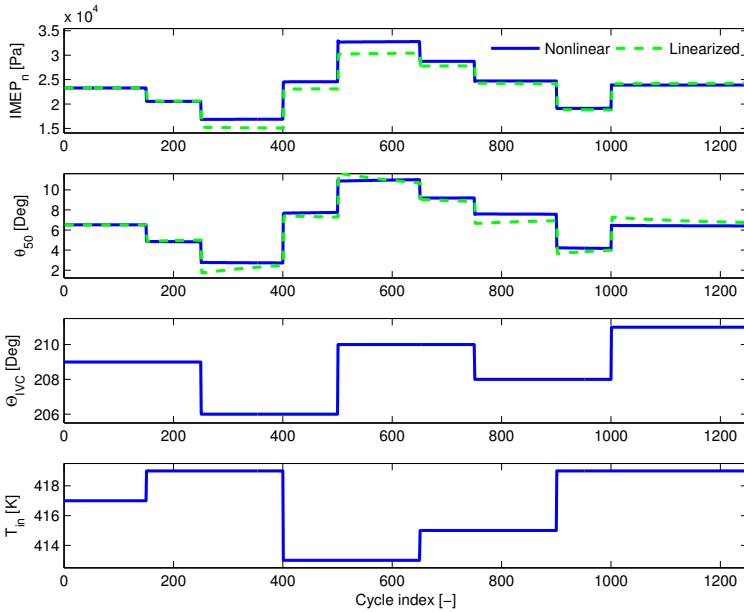

Figure 5.1   IMEP$_n$ and θ_{50} from the nonlinear model and the linearization in response to the control signals θ_{IVC} and T_{in}.

5.3 Control Signals

As mentioned in Chapter 1, there is a wide array of possible control signals for controlling the auto-ignition in HCCI engines. The control signals considered in this work are the crank angle of inlet valve closing and the inlet air temperature, denoted θ_{IVC} and T_{in} respectively.

Inlet Valve Closing

The effect of changing θ_{IVC}, in the framework of the model in Chapter 4, is mainly geometrical by changing the effective compression ratio. Only values between bottom dead center and top dead center are considered, so that a greater value of θ_{IVC} means less compression and later combustion. This introduces a magnitude limitation on the control signal, but it can be changed freely between cycles.

Intake Temperature

Altering the intake temperature affects the pre-compression conditions in the cylinder and a higher intake temperature promotes earlier combustion. Changing the intake temperature is more involved than changing θ_{IVC}. In the experimental setup considered, the intake temperature was originally governed by an electric heater. The electric heater was in turn controlled by a PI-controller and the output of any top-level controller generated the set-point for this controller. The response of this system was fairly slow which showed to be detrimental to the resulting control performance. In the following, two strategies for handling this situation are described.

Model augmentation   One option is to model the dynamics of the intake temperature control loop. This allows the top-level controller to compensate for the dynamics, and also introduces measurements of the actual intake temperature. The heater was modeled as a first order system, so that

$$T_{\text{in}}(k+1) = e^{-1/T_f} T_{\text{in}}(k) + \left(1 - e^{-1/T_f}\right) T_{\text{in}}^r(k) \qquad (5.9)$$

where T_f is the time constant and T_{in}^r is the reference value for T_{in}. Figure 5.2 shows the measured response to a step in desired intake temperature and the response of the first-order approximation in (5.9). It
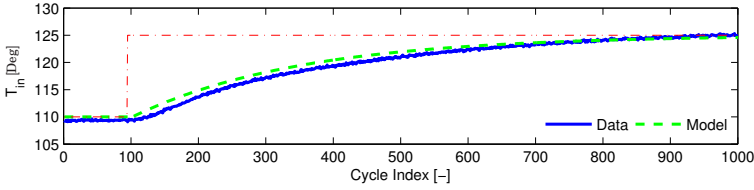
Figure 5.2 Measured and simulated response to a step change in the desired intake temperature. Measurement data by courtesy of M. Karlsson.

should be noted that the time constant of the heater dynamics depends on the tuning of the control loop governing the intake temperature. The heater model was then included in the HCCI model, and the extended model was used for control design. Combining (5.9) and (5.6) yields a third-order system.

$$\left(\begin{array}{c} y(k+1) \\ T_{\text{in}}(k+1) \end{array} \right) = A_e \left(\begin{array}{c} y(k) \\ T_{\text{in}}(k) \end{array} \right) + B_e \left(\begin{array}{c} \theta_{IVC}(k) \\ T^r_{\text{in}}(k) \end{array} \right) \tag{5.10}$$

where

$$A_e = \left(\begin{array}{cc} A & B_{[:,2]} \\ 0 & e^{-1/T_f} \end{array} \right), \quad B_e = \left(\begin{array}{cc} B_{[:,1]} & 0 \\ 0 & 1 - e^{-1/T_f} \end{array} \right) \tag{5.11}$$

This means that the control signal T_{in} is replaced with its reference value.

Fast Thermal Management   During the project, the engine was rebuilt to support fast actuation of the intake temperature. The intake temperature was then governed by two valves, a cooler, and a heater, see Figure 5.3. A similar system was used in [Haraldsson, 2005] and there denoted Fast Thermal Management. The heater power (q_h) could be set as well as the positions of the two valves, denoted α_{HV} and α_{CV} for the heater valve and the cooler valve respectively.

Assuming that the thermodynamic conditions before and after the throttles are approximately equal, the mass flow and pressure after the throttles can be maintained by requiring that the total projected flow area of the two throttles is kept constant. This assumption is not
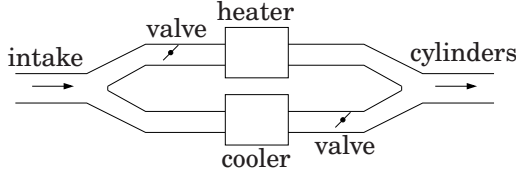
Figure 5.3   Schematic of the fast intake temperature control system.

likely to hold for the individual throttles, but the experiments suggest that the impact on the resulting intake pressure is small. Denote by $\bar{A}_{th}$ the area of each throttle plate. The projected flow area of each plate is then given by

$$A_{HV} = (1 - \cos \alpha_{HV}) \, \bar{A}_{th}, \quad A_{CV} = (1 - \cos \alpha_{CV}) \, \bar{A}_{th} \tag{5.12}$$

The condition of constant projected flow area can be written

$$\bar{A}_{th} = A_{HV} + A_{CV} \tag{5.13}$$

solving for α_{CV} gives

$$\alpha_{CV} = \cos^{-1}(1 - \cos(\alpha_{HV})) \tag{5.14}$$

With this relation between α_{HV} and α_{CV} the intake temperature control system has two inputs (α_{HV} and q_h) and one output (T_{in}). The heater input is relatively slow while the valve has a faster response but a narrower operating range. This makes the system suitable for mid-ranging control [Allison and Isaksson, 1998]. An example of HCCI control using a mid-ranging strategy was presented in [Karlsson *et al.*, 2007]. A block diagram of the mid-ranging control strategy for control of the intake temperature is shown in Figure 5.4. Controller C_1 governed α_{HV} to fulfill $T_{in} = T_{in}^r$ where T_{in}^r is the desired intake temperature. Controller C_2 governed q_h in order to keep α_{HV} at a desired value α_{HV}^r. Choosing α_{HV}^r slightly above the middle of the operating range gave a fairly fast response to changes in desired intake temperature.

The controllers were both of PI-type and manually tuned. Figure 5.5 shows a typical step response for the closed-loop system. Also shown is the intake pressure, which varied less than one percent during the step.
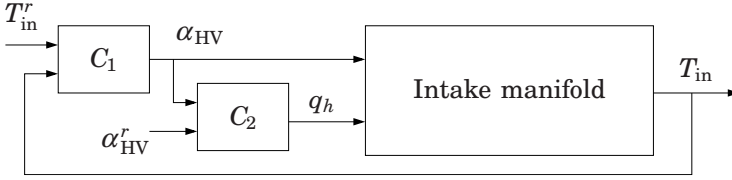
Figure 5.4   Intake temperature control strategy.
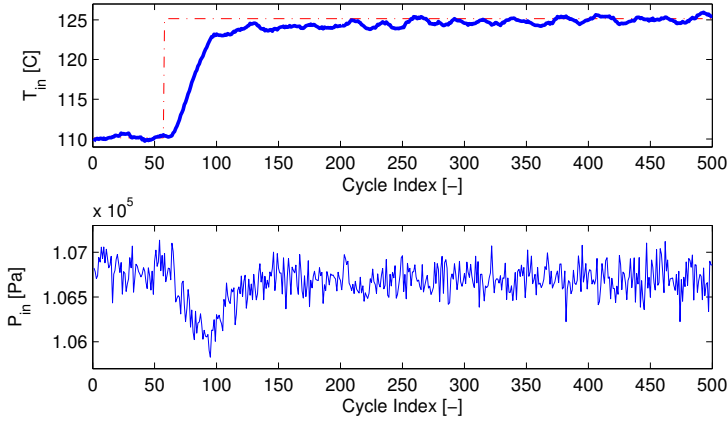
Figure 5.5   Intake temperature control, step response. The bottom plot shows the intake pressure.

It should be noted that there was a certain inertia in the temperature sensor. Anti-windup was implemented to handle power constraints on the heater and bounds on α_{HV}. A lower bound on α_{HV} greater than zero was introduced in order to always maintain a minimum hot flow to avoid damages to the heater.

5.4 Model Predictive Control

Model predictive control was shown to be a suitable control strategy for HCCI [Bengtsson *et al.*, 2006] due to its MIMO-capabilities and its

ability to handle explicit constraints on control signals and outputs. Other control strategies that have been successfully applied to HCCI include PID and LQ control [Bengtsson, 2004; Strandh, 2006; Karlsson, 2008; Haraldsson, 2005] as well as nonlinear control laws [Chiang *et al.*, 2007].

Basic Algorithm

The following review is based on [Maciejowski, 2002].

Consider the cost function

$$J(k) = \sum_{i=1}^{H_p} \mathcal{Y}(i|k) + \sum_{i=0}^{H_u-1} \mathcal{U}(i|k) \tag{5.15}$$

where

$$
\begin{aligned}
\mathcal{Y}(i|k) &= ||\hat{y}(k+i|k) - r(k+i|k)||_Q^2, \\
\mathcal{U}(i|k) &= ||\Delta\hat{u}(k+i|k)||_R^2
\end{aligned}
\tag{5.16}
$$

and $\hat{y}(k+i|k)$ is the predicted output error at time $k+i$ given a measurement at time k, $\Delta\hat{u}(k+i|k)$ is the predicted change in control signal, and $r(k+i|k)$ is the set point at time $k+i$. This is visualized in Figure 5.6. The parameters H_p and H_u define the length of the prediction horizon and the control horizon. The weights Q and R are tuning parameters and may be time-varying. At each sample, the cost function in (5.15) is minimized by determining a sequence of changes to the control signal $\Delta u(k+i|k)$, $i = 0 \ldots H_u - 1$, subject to the constraints

$$
\begin{aligned}
y_{\min} &\leq y(k) \leq y_{\max} \\
u_{\min} &\leq u(k) \leq u_{\max} \\
\Delta u_{\min} &\leq \Delta u(k) \leq \Delta u_{\max}
\end{aligned}
\tag{5.17}
$$

for all k. The first step of the optimal sequence is then applied to the plant and the optimization is repeated in the next step yielding a new optimal sequence [Maciejowski, 2002].

Error-free Tracking

To achieve error-free tracking either a disturbance observer or introduction of integrating states may be adopted [Åkesson, 2006]. The dis-
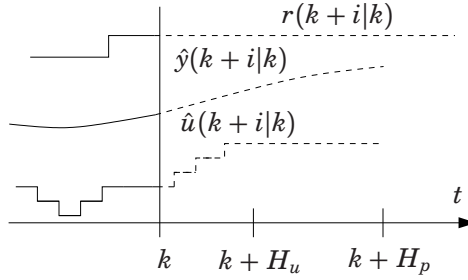
Figure 5.6 Past and future reference, output, and control signal.

turbance observer approach is based on the extended model formulation

$$\begin{pmatrix} x(k+1) \\ v_a(k+1) \\ d(k+1) \end{pmatrix} = \begin{pmatrix} A & 0 & B \\ 0 & I & 0 \\ 0 & 0 & I \end{pmatrix} \begin{pmatrix} x(k) \\ v_a(k) \\ d(k) \end{pmatrix} + \begin{pmatrix} B \\ 0 \\ 0 \end{pmatrix} u(k) \qquad (5.18a)$$

$$y(k) = \begin{pmatrix} C & 0 & 0 \end{pmatrix} \begin{pmatrix} x(k) & v_a(k) & d(k) \end{pmatrix}^T \qquad (5.18b)$$

$$y_m(k) = \begin{pmatrix} C & I & 0 \end{pmatrix} \begin{pmatrix} x(k) & d(k) & v_a(k) \end{pmatrix}^T \qquad (5.18c)$$

where $y_m(k)$ are the output measurements and $y(k)$ are the controlled outputs. For further details, see [Åkesson and Hagander, 2003].

Disturbance Modeling

With knowledge about the properties of the output measurement noise, an additional extension is possible [Bemporad *et al.*, 2004]. The state vector is then extended with a system driven by white noise and the output of this system is added to the measured output. For prediction purposes, the noise input is assumed zero over the prediction horizon. This approach is applied in Chapter 7.

5.5 Discussion

The change of states presented in Section 5.1 removes the need for using an observer for estimating the temperature states. However, due
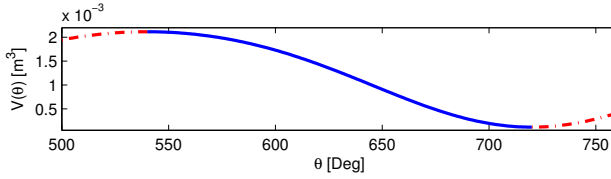
Figure 5.7 The volume $V(\theta)$ plotted against the crank angle θ. The dashed parts are outside the allowed values of θ_{IVC}.

to measurement noise, filtering was still applied in the experiments. This also allows for using a disturbance observer to achieve error-free tracking and estimating the states of the output disturbance subsystem.

The linearization introduces some additional model errors when operating far from the linearization point. One way of handling this is the use of several linearizations. This is employed in Chapter 6. The poles of the linearized system around the nominal operating point were in approximately 0.03 and 0.96. When changing linearization point, the main variation was in the system gain rather than in the pole locations. Parts of the model are better suited for linearization than others. A possible improvement could be achieved by changing the input signal from θ_{IVC} to the desired volume $V(\theta_{\mathrm{IVC}})$. Given a desired volume, the corresponding θ_{IVC} could be determined from (4.11), since the function $V(\theta)$ is injective for θ between bottom dead center and top dead center, as illustrated in Figure 5.7. The resulting system would be of Hammerstein type. In [Karlsson *et al.*, 2007] system identification was used to estimate the nonlinear relation between inlet valve closing and combustion phasing over a larger interval.

Two ways of handling the slow heater dynamics were presented. The model augmentation strategy should be applicable also to other actuators that include relevant dynamics that are difficult to incorporate in the nominal model formulation, such as a long-route EGR system. For the Fast Thermal Management, a mid-ranging control strategy was chosen and manually tuned. It is possible that a model-based control design could improve the closed-loop performance. Combined with estimation of the flows past the valves this would also extend the operating range as smaller values of α_{HV} would be admissible without

risking damages to the heater. Another option would be removing the non-zero lower bound on α_{HV} and instead setting $q_h = 0$ when α_{HV} goes below a threshold. The intake temperature control could also be included in the top-level predictive controller.

6

Control of Combustion Phasing and Work Output

This chapter presents results on model-based control of ignition timing and work output in an HCCI engine. Linearizations of the model in Chapter 4 were used to design model predictive controllers for simultaneous control of the ignition timing and the indicated mean effective pressure by varying the inlet valve closing and the intake temperature. The performance of the resulting controller was evaluated by simulating the nonlinear model and two possible extensions were developed. An extended controller was validated on a real engine. Studies of combined control of more than one HCCI output were presented in [Bengtsson *et al.*, 2006; Shaver *et al.*, 2006b]. An approach for decoupled control of peak cylinder pressure and ignition timing was presented in [Shaver *et al.*, 2005].

6.1 Control Design

The linear model (5.6) was used to generate predictions in the MPC strategy. To ensure error-free tracking explicit integrator states were added to the linear model [Åkesson, 2006]. Constraints were added to the outputs mainly to limit deviations in combustion phasing, while the constraints on the control signals were introduced based mainly on the limitations of the actuators but also to avoid excitation of unmodeled effects related, e.g., to the gas exchange process. Suitable values for the prediction and control horizons were determined from simulation.

6.2 Controller Evaluation

This section presents the evaluation of the nominal controller and discusses two possible extensions.

Nominal Controller Performance

The simulated response using the nominal controller during a series of step changes in the reference values is shown in Figure 6.1. The controller followed the reference trajectory for both outputs. There were some transients in θ_{50} during the step changes in IMEP_n. These could be partly diminished by further tuning of the controller. However, as shown in the next section, using a controller based on the piece-wise linear approximation suggested in Section 5.2 reduces the transients substantially.
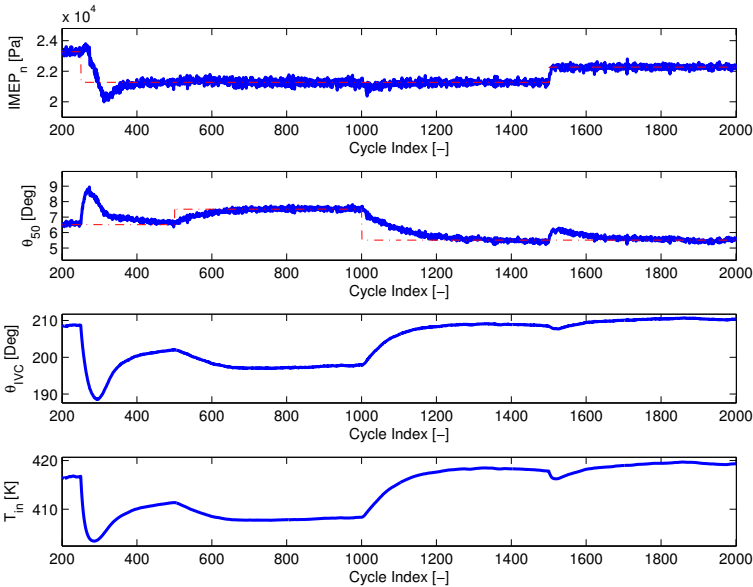

Figure 6.1 Simulated IMEP_n, θ_{50}, and control signals θ_{IVC} and T_{in} for the nominal model predictive controller.

Piece-wise Linear Approximation

As noted in Section 5.2, the fit of the linear approximation is deteriorating with increasing distance from the linearization point. Figure 6.2 shows the simulated response to the nominal model predictive controller and to a switched controller based on a piece-wise linear approximation using three regions. The weights and prediction parameters were the same for both controllers. The switched controller utilized a more accurate dynamic model and yielded better performance. The transients in θ_{50} during the steps in IMEP_n were reduced and the overall response was faster.

Figure 6.2 Simulated IMEP_n, θ_{50}, and control signals θ_{IVC} and T_{in} for the nominal model predictive controller and the switched controller.

Actuator Modeling

Introducing the dynamics of the heater had a drastic effect on the control results. This is partly due to the predictions being made with

an incorrect intake temperature. A controller was designed based on the extended model in (5.10) and compared to one based on the nominal model. As measurement of T_{in} is possible, the control actions were based on the actual intake temperature. In order to obtain reasonable tracking of combustion phasing using the nominal model, the penalty on $IMEP_n$ was reduced and that on the intake temperature control signal was increased. The controller based on the extended model controlled both outputs relatively fast in simulation, as shown in Figure 6.3.
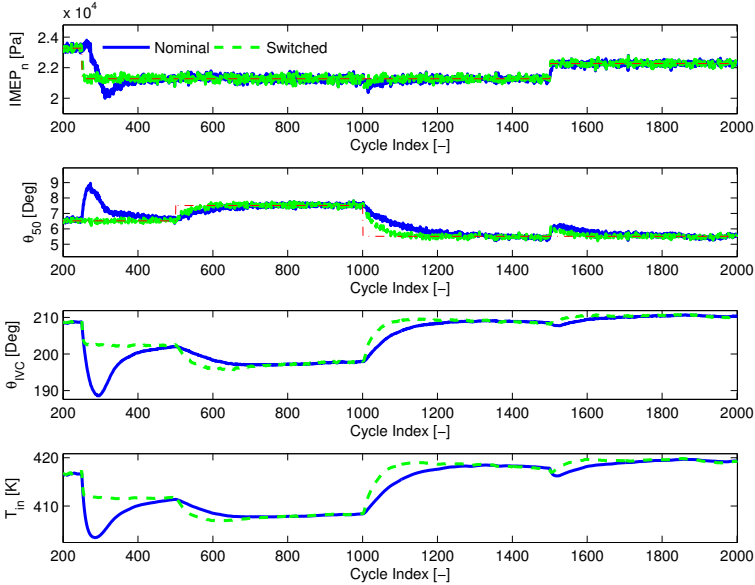

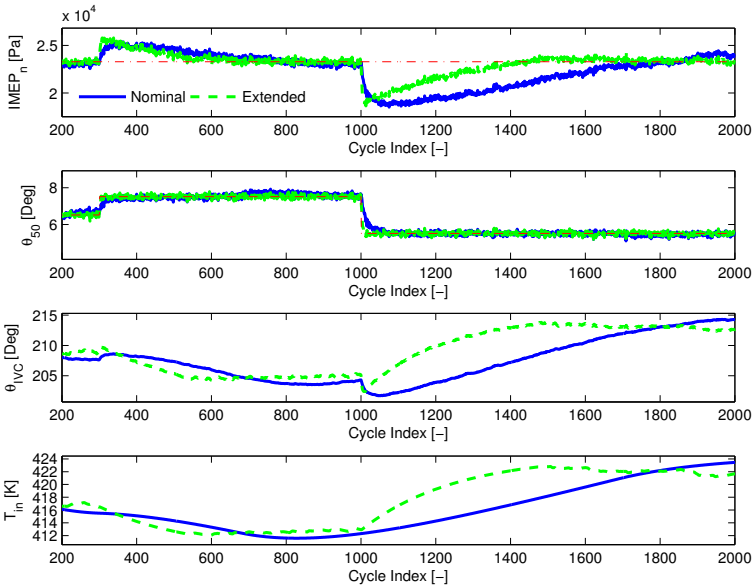**Figure 6.3** Simulated $IMEP_n$, θ_{50}, and control signals θ_{IVC} and T_{in} for the nominal model predictive controller and the controller based on the extended model.

Experimental Validation

The extended controller, including the actuator model, was used to control the metal engine described in Section 3.2. The controller was implemented in Simulink and converted to C-code using Real Time

Workshop. The injected fuel energy was 1400 J and no exhausts were recycled.

As the simulations used a model calibrated against the optical engine described in Section 3.1, re-calibration was needed. Aside from this, however, only little time was spent tuning the controller.

Figure 6.4 shows experimental results during step changes in the set-point for θ_{50}. The controller followed the set-point changes with a slight overshoot.
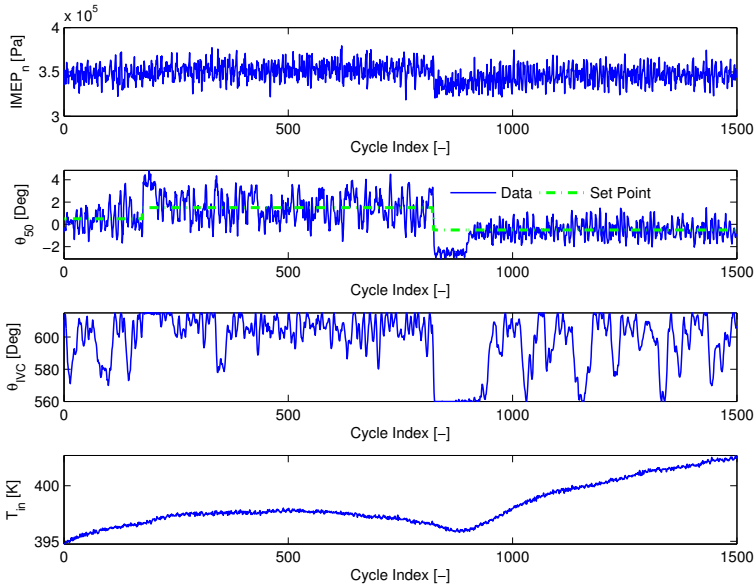
Figure 6.4   Experimental $IMEP_n$, θ_{50}, and control signals θ_{IVC} and T_{in} for the extended controller on the real engine.

6.3 Discussion

The piece-wise linear approximation of the model yielded good results in simulation which suggests that the approach should be pursued further. Some theoretical questions remain, such as how to choose the

linearization points. In this work the switches were made solely based on the θ_{50}-measurement and the linearization points were chosen in an *ad hoc* fashion. However, the approach simplifies the control design compared to using nonlinear methods while improving the model precision. Introducing a simple model of the intake heater dynamics enabled simulation of a more realistic engine model for the control design. It also introduced measurements of the actual intake temperature in the extended controller. An important aspect of this setup is that the output predictions are based on a more correct state estimate. The experimental results show qualitative agreement with the simulations. The resulting control performance could most likely be improved substantially with some additional tuning of the controller. A slight overshoot in θ_{50} was noted and Figure 6.4 shows that the variance was larger with later combustion phasing.

6.4 Conclusion

A cycle-resolved, physical model of HCCI was used to design model predictive controllers augmented with integrating states. The inclusion of cylinder wall temperature dynamics in the model provided a physically well-founded link between engine cycles when only small amounts of residuals were captured in the cylinder. A change of coordinates was introduced, enabling the measured outputs to be used as states. A linearized version of the two-input, two-output HCCI model was used to generate predictions in the MPC strategy. The performance of the resulting controller was evaluated in simulation and possible extensions were discussed. An extended version of the controller was experimentally validated on a real engine.

7

Experimental Evaluation

This chapter presents a detailed experimental investigation of the properties of the closed-loop system. In contrast to Chapter 6, the only controlled output was θ_{50}, while IMEP_n was used as a measurement. The motivation for not controlling IMEP_n is that the impact of the considered control signals is fairly small. As the results will show, the robustness towards changes in the amount of fuel was quite good, indicating that a simple controller governing the fuel injection could be added. The fast thermal management system described in Section 5.3 was used, so that the actuator model used in Chapter 6 was no longer needed. The results were evaluated in terms of response time, robustness towards disturbances, and combustion phasing variance. A fast response to combustion phasing set-point changes can be critical to avoid—e.g., misfire or too high peak pressures during certain load changes. To this purpose, focus was on the output variance in steadystate. The effects of altering the prediction and control horizons in the MPC were also investigated with respect to performance and computation time.

7.1 Experimental Conditions

The experiments were performed on the metal engine described in Section 3.2. Due to technical circumstances, four of the cylinders (Cylinder 1, 3, 5, and 6) were operated. The inlet valve closing of each cylinder was governed by four identical controllers while the intake temperature was governed only by Cylinder 5. The main focus of the experiments

were on this cylinder, some multi-cylinder results are presented in Section 7.3. The mid-ranging control strategy for T_{in} was implemented in C++ while the predictive controllers were implemented in Simulink and compiled using Real-Time Workshop. The injected fuel energy was 1400 J and no exhausts were recycled, yielding approximately 3.5 bar $IMEP_n$ in all experiments. When evaluating the robustness towards disturbances the engine speed, the fuel energy, and the amount of recycled exhaust gases were varied.

7.2 Control Design

The linear model in (5.6) was used to generate predictions. As only control of θ_{50} was the objective, there was no penalty on $IMEP_n$, but it was used as a measurement. A small weight was added to penalize $\theta_{IVC}^r - \theta_{IVC}$, where θ_{IVC}^r is the set-point for the control signal, to obtain a slight mid-ranging effect as there are several combinations of control signals that achieve the same output. To avoid excitation effects related to the gas exchange, θ_{IVC} was restricted to $\theta_{IVC} \in [550, 620]$. The inlet temperature was restricted to $T_{in} \in [110, 135]$. To obtain error-free tracking, a disturbance observer [Åkesson and Hagander, 2003] was used.

7.3 Experimental Results

A typical response to a sequence of steps with increasing amplitude is shown in Figure 7.1. The response time was less than 20 cycles for all steps. The intake temperature changed only slightly until the final step, where the inlet valve reached its constraint.

Statistical Properties

The output variance increased notably with later combustion phasing, see Figure 7.2 which shows the steady-state output standard deviation plotted against the θ_{50}-reference.
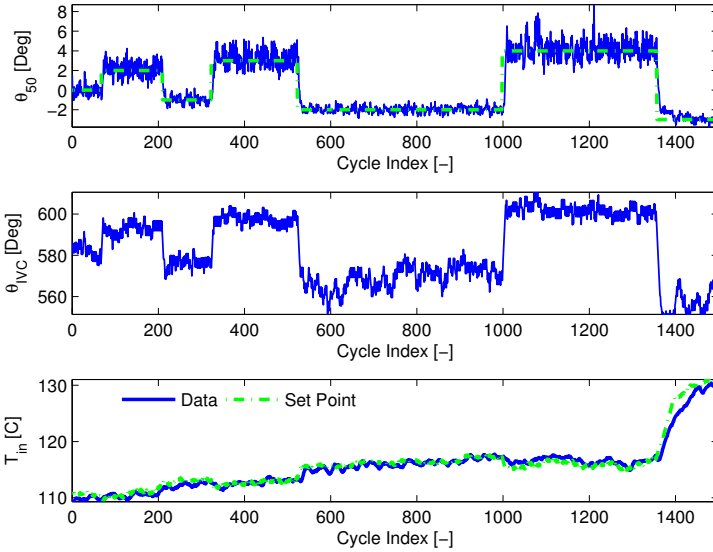
Figure 7.1   Response to steps of increasing amplitude. All set-point changes were accomplished within 20 cycles.
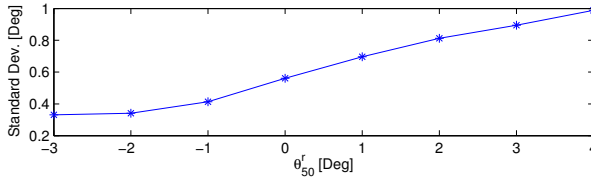
Figure 7.2   Output standard deviation plotted against the set-point for θ_{50}.

Disturbance Modeling   In an attempt to reduce the steady-state output variance at the later combustion phasing, a disturbance model was identified. The model residuals were formed as

$$e_m(k) = \theta_{50}(k) - \hat{\theta}_{50}(k) \tag{7.1}$$

where $\hat{\theta}_{50}(k)$ is the output of the linearized model in response to the input signals. Measurement data from steady-state operation was used. A stochastic realization was found using a subspace-based algorithm

[Johansson, 1993]. There was a distinct gap in magnitude after the first singular value of the identified subspace, indicating that a first-order model was sufficient. A model on the following form was obtained

$$
\begin{array}{rcl}
e_x(k+1) & = & ae_x(k) + Kv(k) \quad\quad\quad\quad (7.2a) \\
e_m(k) & = & Ce_x(k) + v(k) \quad\quad\quad\quad\quad (7.2b)
\end{array}
$$

where e_x is the state and $v(k) \in \mathcal{N}(0, R_e)$.

Extended Controller   The model in (5.6) was extended with the disturbance model in (7.2), yielding

$$
\begin{array}{rcl}
x(k+1) & = & Ax(k) + Bu(k) \quad\quad\quad\quad\quad (7.3a) \\
e_x(k+1) & = & ae_x(k) + Kv(k) \quad\quad\quad\quad\quad (7.3b) \\
y(k+1) & = & x(k) + Ce_x(k) + v(k) \quad\quad\quad (7.3c)
\end{array}
$$

A controller was designed based on the extended model using the same design parameters as for the nominal controller. For set-points close to $\theta_{50}^r = 0$ there was no significant reduction in the output variance. However, for $\theta_{50}^r = 4$ the output variance was reduced by almost 10%. A comparable reduction was achieved by replacing the nominal linear model with a new linearization performed around this set-point.

Robustness Towards Disturbances

The robustness towards disturbances in the amount of fuel, the engine speed, and the amount of recycled exhaust gases was investigated experimentally. Figure 7.3 shows the response as disturbances were added sequentially. At cycle 200 the engine speed was increased from 1200 rpm to 1400 rpm. The injected fuel energy was reduced from 1400 J to 1200 J at cycle 700. Finally, the amount of recycled exhaust gases (EGR) was increased from approximately 0% to 30% at cycle 1350. The bottom plot shows IMEP_n which reflects the impact of the disturbances in engine speed and fuel energy. The combustion phasing was maintained relatively well through the whole sequence.

Prediction Horizons

A prediction horizon of 5 and a control horizon of 2 was used in the nominal controller. The effects of increasing the horizons were evaluated in terms of control performance and computation time for each
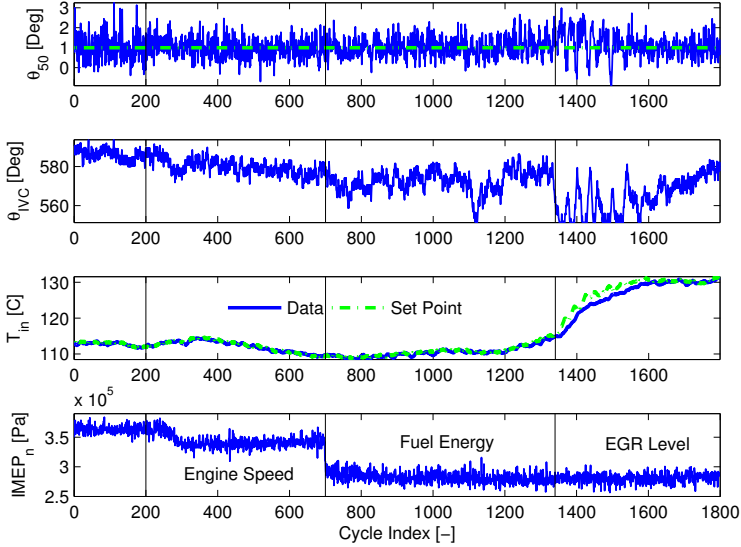
Figure 7.3 Response to disturbances in the engine speed, the amount of injected fuel, and the amount of EGR. $IMEP_n$ is included to visualize the disturbances in engine speed and fuel energy.

cycle. Table 7.1 shows the average computation time measured in processor clock cycles normalized by the largest average. As expected, the computation time grows mainly with the choice of control horizon. The most demanding setting tested, $H_p = 30$ and $H_u = 15$, had a computation time almost sixty times longer than that of $H_p = 5$, $H_u = 2$. However, in terms of control results, the controllers performed practically identically both in terms of response time and output variance.

Multi-Cylinder Control

As previously mentioned, Cylinders 1, 3, 5, and 6 were operated in the experiments and the controller for Cylinder 5 governed the intake temperature. The response to a series of step changes in the set-point for θ_{50} is shown in Figure 7.4. The θ_{IVC}-values requested by the controllers showed a large spread. The variance is slightly higher and response time longer for Cylinder 1.

Table 7.1   Computation time for different choices of prediction and control horizons.

H_p	H_u	CPU Cycles (relative)
5	2	1.0000
10	2	1.0059
7	3	1.5882
10	4	2.6000
15	6	5.8647
15	8	13.3294
20	10	26.0412
30	15	58.8235

Figure 7.4   Response to step changes in the set-point for θ_{50} for Cylinders 1, 3, 5, and 6. The controller for Cylinder 5 governed the intake temperature.

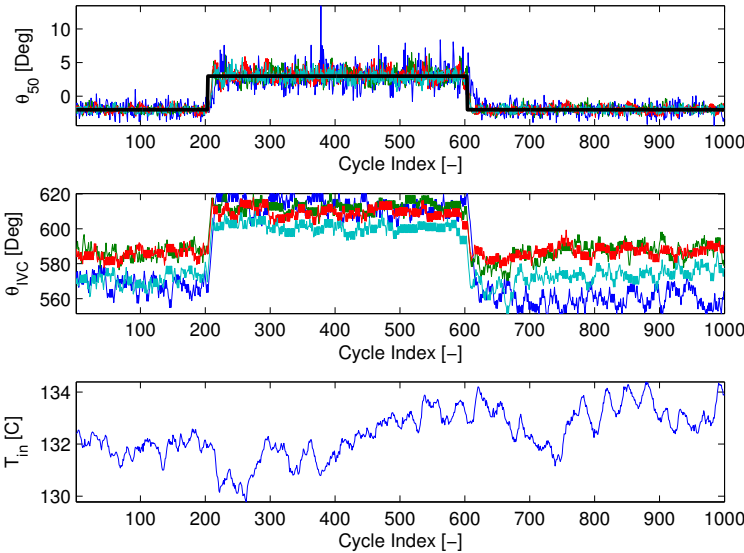**Figure 7.5** Response to step changes in the set-point for θ_{50} for Cylinders 1, 3, 5, and 6. The controller for Cylinder 5 governed the intake temperature.
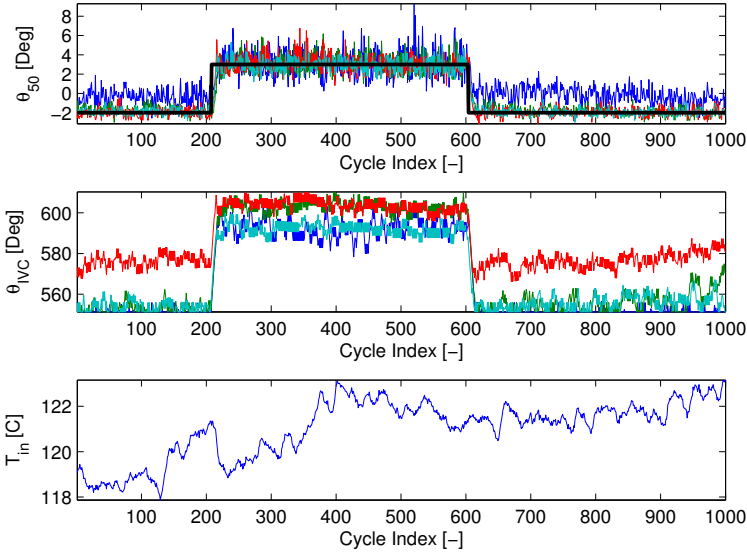
Figure 7.5 shows the same set-point sequence but with different initial values where the intake temperature was lower. In this case tracking is poor for Cylinder 1 and only θ_{IVC} for Cylinder 5 returns to its desired value.

7.4 Discussion

The closed-loop system showed a fairly short response time. For step changes of a few degrees around the linearization point in θ_{50} the response time was approximately ten cycles. Only the larger steps (e.g., from -2 to 4 and from 4 to -3 in Figure 7.1) took around 15 cycles, which compares well with previously published results [Blom *et al.*, 2008; Bengtsson *et al.*, 2007]. The inlet valve closing showed to be a sufficient control signal in many operating points. An additional control signal is, however, needed to extend the range of the controller.

This is apparent, e.g., in the end of Figure 7.1 and during the EGR-disturbance in Figure 7.3.

The output variance under closed-loop control increased with later combustion phasing, as shown in Figure 7.2. As the variance could be reduced either by introducing a disturbance model or by using a linearization made closer to the operating point, the cause seems to be a combination of physical effects and model errors. The use of several linearizations improved the simulated results in Chapter 6 and the observations made here further promotes the strategy. Around top dead center the output variance was relatively low in all cases. This could be partially explained by the operating procedure. As there is no trapping of hot residuals, the dependence on the charge temperature of the previous cycle is weakened, giving the control signals greater impact.

The closed-loop system showed good robustness to disturbances in engine speed, fuel amount, and EGR level. The EGR seems to have the greatest impact on θ_{50} and there was a clear transient occurring in response to the increase. A likely cause for this is that the thermal properties of the charge are altered by increasing the amount of burned gas. Also, as seen in Figure 7.3, the change in EGR is not reflected in $IMEP_n$, which is used as measurement in the controller.

The results suggest that fairly short control- and prediction horizons are sufficient. This might not hold true during other circumstances and model formulations. It is, however, promising that good control results can be achieved with a relatively small computational effort.

The initial multi-cylinder control results seem promising. There is, however, a fairly wide spread in the required θ_{IVC} for the cylinders. This is likely due to variations in the individual cylinders as well as their positions in the engine block. The controller for Cylinder 1 nearly saturated at the final set-point in Figure 7.4 and all controllers except that for Cylinder 5 saturated in Figure 7.5. The situation is similar to that in [Karlsson *et al.*, 2007] where a long-route EGR-system was used together with VVA. Both the long-route EGR level and the intake temperature are global variables shared by all cylinders. The solution adopted in [Karlsson *et al.*, 2007] was to use the mean value of the EGR-levels requested by each controller, which should be suitable for the intake temperature in this setting. However, in Figure 7.5 it is apparent that a single cylinder can have very individual thermal charac-

teristics. Also, these characteristics are not necessarily static, as seen by comparing Figures 7.4 and 7.5. A possible improvement could be to attempt to model the flow dynamics in the intake to handle these variations.

7.5 Conclusion

Model predictive control of the combustion phasing in an HCCI engine using a physical model was investigated. To obtain fast control of the intake temperature, Fast Thermal Management was implemented using mid-ranging control. The robustness of the controller was investigated by introducing disturbances in the engine speed, the amount of fuel, and the amount of cooled recycled exhaust gases. The output variance was investigated and a disturbance model was included in the controller, yielding a decrease in the steady-state variance at certain operating points. A comparable decrease was, however, achieved by using a linearization performed closer to the operating point, showing the advantage of physically motivated models. The effects of changing prediction and control horizons in the controller were investigated both in terms of performance and computation time. The results suggest that fairly short horizons are sufficient.

8

Conclusion and Future Work

A cycle-resolved HCCI model including cylinder wall temperature dynamics was presented. This yields a second-order model intended for control design that captures the main dynamics of the interaction between the gas charge and the cylinder wall. The cylinder wall temperature dynamics provide a reasonable explanation for the cycle-to-cycle dynamics in HCCI when only small amounts of residuals are trapped in the cylinder. However, if the engine is operated with high levels of recycled, hot, exhaust gases it is not certain that this effect is of great importance. In some cases, modeling of, e.g., the intake system to capture variations in the intake pressure can be important. In this work no such modeling was included as the operating principle did not generate any major pressure variations. There is a distinct trade-off between model complexity and the number of physical effects that can be described.

An important part of HCCI modeling is the prediction of auto-ignition. While Arrhenius-type integrals provide fairly good prediction accuracy, the structure of the integrals increase model complexity considerably. As linear models often are used for control design, using linearizations of these expressions seems to be a reasonable choice. However, as several variables affect auto-ignition, the linearizations themselves easily become complex. A related issue is model calibration. The methods used in Chapter 4 are fairly straight forward but come with no guarantees of convergence. It would be beneficial to have

a systematic method which requires as little user interaction as possible to simplify porting of the model.

Both simulated and experimental control results suggest a noticeable performance increase from the use of several linearizations. In the simulation study, a Linear Parameter Varying model formulation was used and improved the dynamic performance. In the experimental study the steady-state output variance was in focus and a new linearization yielded the same variance reduction as did an identified disturbance model in certain operating points. The selection of linearization points and switching strategy would likely benefit from a systematic selection strategy. For implementing a switched control structure, explicit MPC [Bemporad *et al.*, 2002] could be suitable to reduce the online computational burden. The use of an identified disturbance model would also be interesting to investigate further. An adaptive scheme where the disturbance model is updated during operation is conceivable. The approach has similarities with subspace predictive control [Favoreel and de Moor, 1998], but the nominal, physical model would be left unchanged, similar to the model refinement strategies in [Palanthandalam-Madapusi *et al.*, 2005].

A more practical issue is that the use of the intake temperature as control variable requires some form of heating. While an electric heater was used in the presented work, this might not be feasible in a production setting. A possibility would be using residual gas trapping, or using the exhaust gases to heat the intake air.

9

Bibliography

Åkesson, J. (2006): "MPCtools 1.0—Reference Manual." Technical Report ISRN LUTFD2/TFRT--7613--SE. Department of Automatic Control, Lund Institute of Technology, Sweden.

Åkesson, J. (2007): *Tools and Languages for Optimization of Large-Scale Systems*. PhD thesis ISRN LUTFD2/TFRT--1081--SE, Department of Automatic Control, Lund University, Sweden.

Åkesson, J. and P. Hagander (2003): "Integral action – A disturbance observer approach." In *Proceedings of European Control Conference*. Cambridge, UK.

Allison, B. J. and A. J. Isaksson (1998): "Design and performance of mid-ranging controllers." *Journal of Process Control*, **8:5-6**, pp. 469–474.

Aoyama, T., Y. Hattori, J. Mizuta, and Y. Sato (1996): "An experimental study on premixed-charge compression ignition gasoline engine." *SAE Technical Papers*, **No 960081**.

Bemporad, A., M. Morari, V. Dua, and E. N. Pistikopoulos (2002): "The explicit linear quadratic regulator for constrained systems." *Automatica*, **No 38**, pp. 3–20.

Bemporad, A., M. Morari, and N. L. Ricker (2004): *Model Predictive Control Toolbox. User's Guide*. The MathWorks Inc.

Bengtsson, J. (2004): *Closed-Loop Control of HCCI Engine Dynamics*. PhD thesis ISRN LUTFD2/TFRT--1070--SE, Department of Auto-

matic Control, Lund Institute of Technology, Lund University, Sweden.

Bengtsson, J., M. Gäfvert, and P. Strandh (2004): "Modeling of HCCI engine combustion for control analysis." In *IEEE Conference in Decision and Control (CDC 2004)*, pp. 1682–1687. Bahamas.

Bengtsson, J., P. Strandh, R. Johansson, P. Tunestål, and B. Johansson (2006): "Model predictive control of homogeneous charge compression ignition (HCCI) engine dynamics." In *2006 IEEE International Conference on Control Applications*. Munich, Germany. pp. 1675-1680.

Bengtsson, J., P. Strandh, R. Johansson, P. Tunestål, and B. Johansson (2007): "Hybrid modelling of homogeneous charge compression ignition (HCCI) engine dynamic—A survey." *International Journal of Control*, **80:11**, pp. 1814–1848.

Blom, D., M. Karlsson, K. Ekholm, P. Tunestål, and R. Johansson (2008): "HCCI engine modeling and control using conservation principles." *SAE Technical Papers*, **No 2008-01-0789**.

Canova, M., R. Garcin, S. Midlam-Mohler, Y. Guezennec, and G. Rizzoni (2005): "A control-oriented model of combustion process in a HCCI diesel engine." In *Proc. 2005 American Control Conference*, pp. 4446–4451. Portland, OR, USA.

Chang, J., O. Güralp, Z. Filipi, D. Assanis, T.-W. Kuo, P. Najt, and R. Rask (2004): "New heat transfer correlation for an HCCI engine derived from measurements of instantaneous surface heat flux." *SAE Technical Papers*, **No 2004-01-2996**.

Chang, K., G. A. Lavoie, A. Babajimopoulos, Z. S. Filipi, and D. N. Assanis (2007): "Control of a multi-cylinder HCCI engine during transient operation by modulating residual gas fraction to compensate for wall temperature effects." *SAE Technical Papers*, **No 2007-01-0204**.

Chauvin, J., O. Grondin, E. Nguyen, and F. Guillemin (2008): "Real-time combustion parameters estimation for HCCI-diesel engine based on knock sensor measurement." In *Proc. 17th IFAC World Congress*, pp. 8501–8507. Seoul, Korea.

Chiang, C. and A. Stefanopoulou (2006): "Sensitivity analysis of combustion timing and duration of homogeneous charge compression ignition (HCCI) engines." In *Proc. 2006 American Control Conference*, pp. 1857–1862. Minneapolis, Minnesota, USA.

Chiang, C.-J., A. G. Stefanopoulou, and M. Jankovic (2007): "Nonlinear observer-based control of load transitions in homogeneous charge compression ignition engines." *Control Systems Technology, IEEE Transactions on*, **15:3**, pp. 438–448.

Christensen, M., A. Hultqvist, and B. Johansson (1999): "Demonstrating the multi fuel capability of a homogeneous charge compression ignition engine with variable compression ration." *SAE Technical Papers*, **No 1999-01-3679**.

Favoreel, W. and B. de Moor (1998): "SPC: Subspace predictive control." Technical Report 98-49. Katholieke Universiteit, Leuven.

Haraldsson, G. (2005): *Closed-Loop Combustion Control of a Multi Cylinder HCCI Engine using Variable Compression Ratio and Fast Thermal Management*. PhD thesis ISRN LUTMDN/TMHP--05/1028--SE, Department of Heat and Power Engineering, Lund Institute of Technology, Lund University, Sweden.

Heywood, J. B. (1988): *Internal Combustion Engine Fundamentals*. McGraw-Hill International Editions, New York.

Hillion, M., J. Chauvin, and N. Petit (2008): "Controlling the start of combustion on an HCCI diesel engine." In *Proc. 2008 American Control Conference*, pp. 2084–2091. Seattle, Washington, USA.

Hohenberg, G. F. (1979): "Advanced approaches for heat transfer calculations." *SAE Technical Papers*, **No 79-08-25**.

Ishibashi, Y. and M. Asai (1979): "Improving the exhaust emissions of two-stroke engines by applying the activated radical combustion." *SAE Technical Papers*, **No 790501**.

Johansson, R. (1993): *System Modeling and Identification*. Prentice Hall, Englewood Cliffs, New Jersey.

Karlsson, M. (2008): "Control structures for low-emission combustion in multi-cylinder engines."

Licentiate Thesis ISRN LUTFD2/TFRT--3243--SE. Department of Automatic Control, Lund University, Sweden.

Karlsson, M., K. Ekholm, P. Strandh, R. Johansson, P. Tunestål, and B. Johansson (2007): "Closed-loop control of combustion phasing in an HCCI engine using VVA and variable EGR." In *Fifth IFAC Symposion on Advances in Automotive Control*. Monterey, USA.

Maciejowski, J. (2002): *Predictive Control with Constraints*. Prentice-Hall, Essex, England.

Mathworks (2004): *Real-Time Workshop. User's Guide*. The Math-Works Inc.

Najt, P. M. and D. E. Foster (1983): "Compression-ignited homogeneous charge combustion." *SAE Technical Papers*, **No 830264**.

Onishi, S., S. H. Jo, K. Shoda, P. D. Jo, and S. Kato (1979): "Active thermo-atmosphere combustion (ATAC) - a new combustion process for internal combustion engines." *SAE Technical Papers*, **No 790501**.

Palanthandalam-Madapusi, H. J., E. L. Renk, and D. S. Bernstein (2005): "Data-based model refinement for linear and hammerstein systems using subspace identification and adaptive disturbance rejection." In *2005 IEEE Conference on Control Applications*, pp. 1630–1635. Toronto, Canada.

Rakopoulos, C. D., D. C. Rakopoulos, G. C. Mavropoulos, and E. G. Giakoumis (2004): "Experimental and theoretical study of the short term response temperature transients in the cylinder walls of a diesel engine at various operating conditions." *Applied Thermal Engineering*, **No 24**, pp. 679–702.

Rausen, D. J., A. G. Stefanopoulou, J.-M. Kang, J. A. Eng, and T. W. Kuo (2004): "A mean-value model for control of homogeneous charge compression ignition (HCCI) engines." In *Proc. 2004 American Control Conference*, pp. 125–131. Boston, Massachusetts, USA.

Ravi, N., M. J. Roelle, A. F. Jungkunz, and J. C. Gerdes (2006): "A physically based two-state model for controlling exhaust recompression HCCI in gasoline engines." In *Proc. of IMECE'06*. Chicago, Illinois, USA.

Roelle, M. J., N. Ravi, A. F. Jungkunz, and J. C. Gerdes (2006): "A dynamic model of recompression HCCI combustion including cylinder wall temperature." In *Proc. IMECE2006*. Chicago, Illinois, USA.

Särner, G., M. Richter, M. Aldén, A. Vressner, and B. Johansson (2005): "Cycle resolved wall temperature measurements using laser-induced phosphorescence in an HCCI engine." *SAE Technical Papers*, **No 2005-01-3870**.

Shahbakhti, M. and R. Koch (2007): "Control oriented modeling of combustion phasing for an HCCI engine." In *Proc. 2007 American Control Conference*, pp. 3694–3699. New York City, USA.

Shaver, G. M., M. Roelle, and J. C. Gerdes (2005): "Decoupled control of combustion timing and work output in residual-affected HCCI engines." In *Proc. 2005 American Control Conference*, pp. 3871–3876. Portland, Oregon, USA.

Shaver, G. M., M. Roelle, and J. C. Gerdes (2006a): "Modeling cycle-to-cycle dynamics and mode transition in HCCI engines with variable valve actuation." *Control Engineering Practice*, **No 14**, pp. 213–222.

Shaver, G. M., M. Roelle, and J. C. Gerdes (2006b): "A two-input two-output control model of HCCI engines." In *Proc. 2006 American Control Conference*, pp. 472–477. Minneapolis, Minnesota, USA.

Soyhan, H., H. Yasar, H. Walmsley, B. Head, G. Kalghatgi, and C. Sorusbay (2009): "Evaluation of heat transfer correlations for HCCI engine modeling." *Applied Thermal Engineering*, **No 29**, pp. 541–549.

Strandh, P. (2006): *HCCI Operation - Closed Loop Combustion Control Using VVA or Dual Fuel*. PhD thesis ISRN LUTMDN/TMHP--06/1039--SE, Department of Energy Sciences, Lund University, Sweden.

Strandh, P., J. Bengtsson, M. Christensen, R. Johansson, A. Vressner, P. Tunestål, and B. Johansson (2003): "Ion current sensing for HCCI combustion feedback." *SAE Technical Papers*, **No 2003-01-3216**.

Strandh, P., J. Bengtsson, R. Johansson, P. Tunestål, and B. Johansson (2004): "Cycle-to-cycle control of a dual-fuel HCCI engine." *SAE Paper 2004-01-0941*, **SP-1819**, March. SAE International, Homogeneous Charge Compression Ignition (HCCI) Combustion 2004, ISBN: 0-7680-1355-0.

Wilhelmsson, C., A. Vressner, P. Tunestål, B. Johansson, G. Särner, and M. Aldén (2005): "Combustion chamber wall temperature measurement and modeling during transient HCCI operation." *SAE Technical Papers*, **No 2005-01-3731**.

Woschni, G. (1967): "A universally applicable equation for instantaneous heat transfer coefficient in the internal combustion egnine." *SAE Technical Papers*, **No 670931**.

Nomenclature

Symbols

A_a	Arrhenius scaling factor
A_c	Cylinder wall area, [m^2]
α	Molar fraction of exhaust gases
C_v	Gas heat capacity, [J/(kg·K)]
C_p	Cast iron heat capacity [J/(kg·K)]
E_a	Arrhenius activation energy, [J/kg]
ϕ	Equivalence ratio
γ	Specific heat ratio
h_c	Convective heat transfer coeff., [W/(m^2·K)]
k_c	Conductive heat transfer coeff., [W/(m^2·K)]
L_c	Cylinder wall thickness, [m]
M_a	Air molar mass, [kg]
M_f	Fuel molar mass, [kg]
M_p	Combustion products molar mass, [kg]
m	Gas mass, [kg]
m_a	Air mass, [kg]
m_c	Cylinder wall mass, [kg]
m_f	Fuel mass, [kg]
m_p	Combustion products mass, [kg]
n	Arrhenius sensitivity to pressure
n_a	Amount of air, [mol]
n_f	Amount of fuel, [mol]
n_p	Amount of combustion products, [mol]
P_{in}	Intake pressure, [Pa]
Q_{LHV}	Lower heating value of isooctane, [J/kg]
R	Gas constant, [J/(kg·K)]

T	Gas temperature, [K]
T_c	Coolant temperature, [K]
T_{in}	Intake temperature, [K]
T_{iw}	Cylinder wall inner temperature, [K]
T_w	Cylinder wall surface temperature, [K]
θ_{50}	Crank angle of 50% burnt, [rad]
θ_{IVC}	Crank angle of inlet valve closing, [rad]
θ_{TDC}	Crank angle at top dead center, [rad]
V_d	Displacement volume, [m^3]

Acronyms

ABDC	After bottom dead center
ATDC	After top dead center
BBDC	Before bottom dead center
BTDC	Before top dead center
CAD	Crank angle degree
CI	Compression ignition
EGR	Exhaust gas recirculation
FTM	Fast thermal management
HCCI	Homogeneous charge compression ignition
IMEP$_n$	(net) Indicated mean effective pressure, [Pa]
IVC	Inlet valve closing
LQ	Linear quadratic
MPC	Model predictive control
PID	Proportional integral derivative
SI	Spark ignition
TDC	Top dead center
VVA	Variable valve actuation

Author(s)	*Supervisor*
Anders Widd	Rolf Johansson
	Per Tunestål
	Per Hagander

Title and subtitle
Predictive Control of HCCI Engines using Physical Models

Abstract

Homogeneous Charge Compression Ignition (HCCI) is a promising internal combustion engine concept. It holds promise of combining low emission levels with high efficiency. However, as ignition timing in HCCI operation lacks direct actuation and is highly sensitive to operating conditions and disturbances, robust closed-loop control is necessary. To facilitate control design and allow for porting of both models and the resulting controllers between different engines, physics-based mathematical models of HCCI are of interest.

This thesis presents work on a physical model of HCCI including cylinder wall temperature and evaluates predictive controllers based on linearizations of the model. The model was derived using first principles modeling and is given on a cycle-to-cycle basis. Measurement data including cylinder wall temperature measurements was used for calibration and validation of the model. A predictive controller for combined control of work output and combustion phasing was designed and evaluated in simulation. The resulting controller was validated on a real engine. The last part of the work was an experimental evaluation of predictive combustion phasing control. The control performance was evaluated in terms of response time and steady-state output variance.

Key words
engine control, HCCI engine, Model Predictive Control

Classification system and/or index terms (if any)

Supplementary bibliographical information

Language	*Number of pages*	*Recipient's notes*
English	78	
Security classification		